Determination of a Clinically Relevant Tissue Phantom for Transcutaneous Ultrasound Stimulation of Piezoelectric Discs for Current Density Applications

By

Anna Norman

Submitted to the graduate degree program in Bioengineering and the Graduate Faculty of the University of Kansas in partial fulfillment of the requirements for the degree of Master of Science.

_____

Chairperson Dr. Elizabeth Friis

_____

Dr. Jennifer Robinson

_____

Dr. Candan Tamerler

Date Defended: August 18, 2021

The Thesis Committee for Anna Norman

Certifies that this is the approved version of the following thesis

Determination of a Clinically Relevant Tissue Phantom for Transcutaneous Ultrasound Stimulation of Piezoelectric Discs for Current Density Applications

_____

Chairperson Dr. Elizabeth Friis

Date Approved: August 30, 2021

Abstract

Ventral hernia repairs, one of the most common surgeries, have a recurrence rate ranging from 24-43% even with the use of a prosthetic mesh. Over 1 million Americans will undergo a hernia repair surgery each year according to the FDA [1]. The number of surgeries and recurrences leads to a burden of an estimated $700 million annually for U.S. hospitals [2, 3]. Many of these complications related to the surgery are a result of poor healing and mesh failure. Many patients report chronic abdominal pain, mesh erosion, and mesh migration [4, 5]. The research solution proposed and ongoing is an electrically active hernia repair mesh. The electrical stimulation generator will consist of a piezoelectric disc connected to a circuit and fully encapsulated in medical grade silicone. The piezoelectric discs will be mechanically stimulated by therapeutic ultrasound through the layers of skin, fat, and muscle. Therapeutic ultrasound has been the chosen mode for mechanical loading as it is readily available and a medically safe application. Previous research has shown therapeutic ultrasound successful in the mechanical stimulation of piezoelectric discs [6]. The use of tissue phantoms is common in imaging ultrasound studies but has not been used in the research of stimulating piezoelectric discs with ultrasound. By comparing the power and voltage output of the same PZT disc with different tissue phantoms the effect of the tissue phantom type on the ultrasound stimulation can be examined. Therefore, the different types of tissue phantoms attenuation and speed of sound difference can be compared to that of porcine tissue to achieve a more clinically relevant tissue phantom for a specific application use. A thickness of 40 mm was chosen based on literature on abdominal wall thickness of hernia repair patients. It was determined that a phantom using Humimic® medical gelatin #0 with the combination of a fiber supplement (Metamucil®) was a reusable phantom that allowed for similar voltage output at a resistance of one kiloohm (the expected electrical resistance of muscle). The determined phantom can be utilized with the single piezoelectric disc for future studies to advance research for an electrically active hernia repair mesh.

Acknowledgements

Dr. Elizabeth Friis

I would like to thank my advisor Dr. Lisa Friis for all the guidance and support throughout my graduate degree. She has been a wonderful guidance to my master's research and professional career throughout these two years.

Dr. Jenny Robinson

I would like to thank Dr. Jenny Robinson for her willingness to help with the hernia repair project and provide helpful guidance for future work. Although my interactions were limited she was always willing to help.

Dr. Candan Tamerler

I would like to thank Dr. Candan Tamerler for her help with the related projects of the Bioreactor and hernia repair mesh. I took several classes from Dr. Tamerler and learned a lot research and presentation wise from an esteemed researcher and professional career.

Dr. Ember Krech

I would like to thank Dr. Ember Krech for all the help she gave me with this project and graduate school. Her willingness to answer questions and spend time troubleshooting was a great help. In addition, her constant encouragement and reassurance was invaluable in getting through graduate school.

My lab mates at the University of Kansas

I would like to thank all those in Dr. Friis' lab during my time at KU. The past summer and before the pandemic were invaluable in terms of being able to brainstorm in lab have constant encouragement. I only wish I was able to have more time in-person with everyone. I'd personally like to thank Tori Drapal, Morgan Riley, Luke Lindemann, Savannah Mosier, Ryan Downing, and Evan Haas for always willing to answer questions and encouragement.

My Family

I would like to thank my family for always being supportive and interested in my work. I could not have done this without all of you.

My husband, Drake Norman

I would like to thank my husband Drake Norman for his endless support and encouragement. His willingness to listen, ask questions, and learn what I was doing was amazing. His constant encouragement and advice on graduate school from his own experience was so helpful even if I didn't always want to hear it. He celebrated all the successes with me and was there for every failure with reassurance.

Table of Contents

List of Figures

List of Tables

List of Equations

Chapter 1: Introduction

1.1 Background and Motivation

Hernia repair surgeries are one of the most commonly occurring surgeries every year according to the FDA. A hernia is classified as a protrusion of an internal organ through muscle, frequently taking place in the abdomen and groin regions. Historically these were fixed by skilled surgeons with the use of special suturing techniques. These open surgeries would use techniques like the Bassini or Marcy repair using the patient's own tissues to strengthen the area [2]. However, over time the use of prosthetic mesh has become more relevant with many surgeons choosing to use mesh for hernia repair [7]. The reason mesh is more prevalent is because it has reduced the recurrence rate of hernias. Although a mesh is often put in place to aid a patient in healing by strengthening the area of the abdominal wall to prevent a recurrence, its placement does not come without a cost. Many patients will complain about chronic pain post-operation and worst case there is adhesion and infection [7]. Even with the risk of more surgeries to fix an adhesion or remove an infected mesh surgeons still opt for mesh because it decreases the recurrence rate especially when used in a laparoscopic surgery [8]. By using mesh in a surgery, surgeons have been able to reduce the national recurrence rate to below 5% [7]. With so many patients affected by hernias each year and an increase in mesh usage it was only a matter of time before problems with mesh would be brought to the forefront of hernia repair.

The main concerns surround inflammation, wound healing, chronic pain, adhesion, and infection [9]. Inflammation affects the healing process and after 2-3 weeks there should be full tissue integration in the mesh. However, if this does not occur there is the risk of a recurrence from tissue tearing and another hernia forming as the mesh is stronger than the surrounding tissue. If they are difficult to heal patients such as diabetics this healing process and thus tissue integration can take much longer and has the potential to reach a plateau. The introduction of biosynthetic meshes have helped address some of the problems but these prosthetics are still in early stages of research and are significantly more costly than the standard mesh and procedure [10]. A biosynthetic mesh is ideal as it is absorbed over time and

replaces the torn tissue with a new regenerated one [10]. Most often these biosynthetic meshes are used when a patient has history of previous infections and are at risk for antibiotic resistance, but their effectiveness against recurrence has not been proven. Many studies address the fact that more research needs to be done to prove their effectiveness. The use of electrical stimulation has been used for wound care treatment for decades [11]. The introduction of electrical stimulation technology to a hernia repair mesh is a novel merging of established technologies to address the problem of healing and tissue integration in hernia repair mesh for the treatment of abdominal hernias.

1.2 Specific Aims

The goal of this research is to determine specific tissue phantoms to be used with the piezoelectric generator to best mimic the tissue for transcutaneous stimulation. A secondary goal is to utilize existing piezoelectric power generation technology to deliver a specified current density to a sputter coated hernia repair mesh to act as an electrically stimulated mesh. Medically safe and readily available ultrasound will be the loading source of the piezoelectric generator. Porcine tissues of specified thickness will be compared to crafted and commercially available tissue phantoms to determine the most clinically relevant tissue phantom to use with medically safe therapeutic ultrasound for transcutaneous stimulation of piezoelectric generator. Although there is research in imaging ultrasound with different tissue phantoms there are not specified phantoms to be used when trying to stimulate an implanted device. To create an implanted device that will be stimulated with ultrasound a phantom that accurately represented the skin, fat, and tissue needs to be designed prior to benchtop testing. The different phantoms will have dissimilar acoustic properties such as speed of sound and attenuation. These parameters will directly impact how much mechanical loading the lead zirconate titanate (PZT) disc receives. A comparison of the effect of the tissue phantom type and porcine samples on the PZT output will be measured in the average power output and root mean square voltage output. This was accomplished by developing a circuit with a resistance sweep to deliver voltage and current to a mesh electrode and utilizing a single PZT disc to supply said voltage. It is hypothesized that a single disc will supply enough current to generate a current

density of at least 85 nA/cm^2 in order to provide enhanced healing [12]. In addition, it is hypothesized that a tissue phantom containing fiber additives such as sugar-free Metamucil® will provide a better model for a porcine tissue that has skin, fat, and muscle all intact for the use in research testing. The use of porcine tissue with all said layers is expected to provide greater overall attenuation to the set ultrasound intensity of 1.0 W/cm^2 and thus the most clinically relevant tissue phantom will also provide sufficient attenuation.

Chapter 2: Background and Literature Review

This chapter provides literature in the current field and surrounding topics addressed in this research and reviews the background.

2.1 History of Hernia Repair

Although there has been speculation and vague accounts of hernias in ancient times, one of the more noted definitions and clearly documented case a ventral hernia is from La Chousse [13]. In his dissertation, de Hernia Ventralis 1721, La Chousse describes it as a different hernia than femoral, inguinal, and umbilical cord accounts. This new type of hernia would continue to be called a ventral hernia by the mid eighteenth century by influential surgeons, Henri Le Dran, Rene de Garengeot and August Gottlieb Richter [13]. However, it was with the dawn of modern surgery starting in 1900 to WWII that saw improvements and the introduction of anesthesia, that allowed for more hernia repair surgeries to be performed [14]. Surgical repair of hernias is the most effective treatment of hernias, but presents its own risks of incisional hernias, reoccurrence, and infection. From 1900-WWII there were three techniques mainly used in the surgical repair of hernias: simple laparoplasty (suturing), organic auto or heteroplasty (grafting), Alloplasty (use of prosthetics) [13]. The method of grafting was used by Kirschner in 1910 and involved heterologous, homologous, and autologous fascia. The autologous having the best results [13]. Loewe, Gibson, and Nuttall would all use autologous for hernia repair, however, they determined post-surgery these grafts provided insufficient results. This was mainly due to the fact that transplanting often results in a time-consuming harvesting and functional deficits at the donor sites and would leave bulges at reconstruction site and high reherniation rates [15]. Although grafting was not a sufficient treatment of hernia repair it did contribute to the precursors for the biological collagen and xenografts used today. There had to be something to improve the surgical hernia repair consistently across all patients. This improvement came in the form a woven or knitted mesh.

2.1.1 Use of Prosthetics

To decrease the risk of reoccurrence of the hernia some surgeons crafted the idea to use a prosthetic to support the tension. They began with using braided silver wire to form meshes, but they were stiff, fragile, and produced toxic sulfur silver on their surfaces [13]. Goepel and Witzelt then modified the mesh to contain braided stainless steel and act as a bridge between the two edges of the rectus muscles and would use two layers to add in strength at times [13]. Douglas and Throckmorton used tantalum gauze, however, the meshes still fragmented and had high infection rates. During WWII the tantalum and steel were designated for military work, thus following the war there was an emergence of plastics. These plastics piqued the interest of surgeons using prosthetics as a possible alternative to the tantalum or stainless-steel mesh. They began with using prefabricated perlon and nylon, but these still fell apart and the perlon caused a terrible inflammatory response when used inside the body. New plastics of polypropylene, polyester, and expanded polytetrafluorethylene (ePTFE) caught the interest of those creating hernia meshes. These 'new plastics' were more promising as a prosthetic use for hernia repair [16, 17]. The development of these meshes have been iterative overtime with the use of additives like impregnated antimicrobials and elements of absorbable mesh or non-adhesion forming substances to create hybrid meshes. And many of the designs of the mesh have experimented with the pore sizes and textures of the material. Over the past several years there has been experimentation to create a cross-over between meshes and grafting with the use of biological materials for meshes. These biological meshes however have their own set of concerns with rejection, absorption, and cost.

2.1.2 Mesh and Suturing Techniques

In parallel with the focus of mesh and materials there has also been an emphasis on the suturing techniques and placement of the mesh for more successful hernia repairs. It is important for the mesh to be able to be easily and effectively used by surgeons and fit within their standard surgical procedures. Depending on the hernia location and severity a surgeon may use a variety of techniques to repair the hernia with the mesh. There are three main methods of mesh placement in literature. The first location of mesh placement in the peritoneal cavity[13] This places the mesh in contact with the viscera if placed in

the position where it becomes adjacent to the bowel. This possibility of high risk erosion is a major drawback to this mesh placement technique [18]. However, in recent years new meshes have been created that are coated to prevent this adhesion, so the technique is still used [13]. The second method uses the mesh by placing it over the abdominal wall closure in the subcutaneous perifascial space. This is considered to be a premuscular on lay technique and was refined and popularized by Chevrel [19]. The third and final method has been adopted as the gold standard for open incisional repair where the mesh is placed over the closed posterior rectus sheath and peritoneum. This method is called a retro muscular sub lay technique and was popularized by Rives and Stoppa [20]. Even though it is seen as the gold standard there still exists limited data and literature to promote this method over the Chevrel on lay repair technique [21] One of the many difficulties surgeon face with abdominal hernia repair is the lack of healthy tissue for the mesh placement or primary closure. The widely used surgical method today is the laparoscopic incisional repair that was first performed by Leblanc in 1991 [22]. This method is always used when possible because it is less invasive without losing precision. Even with the current advancements in mesh developments and improvements in incisional hernia repair surgical techniques there are still reasonable high recurrence rates and often limited success.

2.1.3 Cost of Ventral Hernia Repair

Ventral Hernia repair (VHR) can be a burden to the healthcare system because they have a notably high recurrence and infection rates. It has been noted that there has been little innovation in the ventral hernia repair research area because it is not viewed as a clinical challenge and has minimal impact on healthcare resources. However, Poulose et al. describes from 2011 a review of the cost ventral hernias has to the healthcare system, encouraging the need for more research to improve patients' outcomes and become less of an unnecessary burden on the healthcare system. Poulose examines both inpatient non-federal discharges for VHR from 2001-2006 healthcare cost and utilization project, supplemented with the CDC data from 2006 national survey of ambulatory surgery for outpatient estimates [2]. The costs were then standardized to 2010 US dollars using consumer price index and reported as mean with 95%

confidence intervals [2]. The article states the results of the data show that the number of inpatients increased from 126,548 to 154,278 from 2001-2006 with an even larger increase in the number of outpatients from 193,543 to 348,000. Costs are still rising, but from 2006 the total cost in the US for VHR was $3.2 billion. Which the article concludes by reducing the recurrence rate alone, a cost saving to the US would be $32 million for each 1% in reduction in operations.

The need to reduce the recurrence rate not only to improve patient outcomes and quality of life, but also to better help healthcare costs. Even under optimal conditions the VHs occur in up to 28% of patients who undergo abdominal operations [23, 24]. Even with the use of mesh the recurrence rate is still between 24-43% [25]. The chances of a hernia recurring increases with the increased number of repairs and thus the costs associated because of the surge in number of repairs and complications. Despite there being more technical developments in use of mesh and surgical techniques in literature there is still a wide area of research of VHRs that is lacking. It is important the note the demographics they considered for the data, many of the patients undergoing inpatient were older and a higher proportion woman. The outpatient surgery repairs were mainly paid by private insurers while inpatients mainly funded by Medicare and Medicaid with a mean length of stay for patients being 6 days [2]. These inpatient surgeries had notable incidence of hypertension, chronic lung disease, diabetes, and obesity. Diabetic patients tend to have a more difficult time with soft tissue healing post operation. These harder to heal cases could benefit greatly from an electrically stimulating hernia repair mesh during the initial healing process. An electrically stimulated hernia mesh could accelerate the soft tissue healing of the VHR post operation and improve patient outcomes not only for healthy patients but also those with underlying conditions that have a slower and more complicated healing process.

2.1.4 Synthetic Mesh

Synthetic mesh is the more common method of hernia repair currently. By using the prosthetic of a synthetic mesh as compared to suture technique only the risk of a hernia recurrence decreases. One study found especially for patients with co-morbidities who are at high risk for surgical site hernias and

hernia recurrences the rate was a reduced hernia recurrence for these patients when synthetic mesh was used compared to a bio-synthetic acellular dermal matrix (ADM) mesh [13].

The type of mesh used for this study on electrical stimulation is important as it needs to be clinically relevant, but also meet the needs to be an electrode for electrical stimulation. The study done by Sanbhal et. al explores characteristics of different types of mesh and the consequences that can occur. One thing that is important to note from a mechanical property is all synthetic meshes will have a higher strength than the human abdominal wall. Thus, when there is a hernia recurrence it is the tissue failing again and not the mesh. This can be because the tissue did not fully heal, there was not enough tissue ingrowth, and a number of other scenarios. Nowadays there are a variety of structures of meshes made from synthetic material each having their own mechanical properties pertaining to the material used, pattern of weaving, and surgical techniques for implantation. Most often a mesh with a larger pore size is preferred as that allows for more flexibility, decreased shrinkage, and more tissue in growth. There are even types of mesh that are specially coated in antimicrobial agents to prevent mesh infection. There are three different textile types of mesh: woven, nonwoven, and knitted. With nonwoven being better than woven because of their microporous structure that allows for fibrous tissue ingrowth and less adhesion [26].

Table 1 - Mesh Classifications

Mesh Pore Classifications	Pore Size (mm)
Microporous	<0.1
Small	0.1-0.6
Medium	1.0
Large	1.0-2.0
Very Large	>2.0

Research has also found that pore sizes must be large enough to permit infiltration of blood vessels, macrophages, collagen, and fibroblasts. This needs to be greater than 75 micrometers and anything less favors infection [27]. If they are less than 800 micrometers there is a chance for granulomas. Which is an immune system response to a foreign body where the immune cells group around the mesh

filament. The larger the pore size the less likely for granulomas to bridge and engulf the mesh. Also, since this will be implanted in the abdomen it needs to be flexible and allow for muscle forces while still permitting growth and discourage granulation.

Table 2 - Mesh Classifications by Weight

Mesh Classification	Weight (g/m^2)	Popularity (%)
Ultra-Light	<35	12
Light	≥35 & < 70	30
Standard	≥70 & < 140	44
Heavy	≥140	14

Light weight mesh was chosen because it is more elastic and has a larger pore size. Many surgeons choose light weight mesh for these reasons and because after implantation there is less pain and discomfort because of those characteristics. In addition, the light weight meshes demonstrated better biocompatibility than mid weight or heavy weight mesh after post implantation 14 and 28 days [28].

2.1.5 Mesh Concerns: Infection and Shrinkage

The risk of infection and shrinkage are critical factors to consider with mesh implementation. The risk of infection as mentioned before can be detoured with porosity of mesh. Currently, there is a realm of research in mesh coatings to prevent and treat infections with the use of antimicrobial and PEG coatings. Some form of shrinkage will occur but minimizing this is important for patient comfort and healing. The synthetic mesh is a foreign body revving up the inflammatory reaction of the body. This inflammation causes a scar plot formation which will result in shrinkage of the mesh because the abdominal wall has increased stiffness [29].The main factors explored and seen affecting shrinkage are moisture content of the filament, machine parameters and knotted structure. In addition, some material may generate a higher inflammatory response than others. If extensive shrinkage occurs, then the repaired area will experience too much stress and could result in recurrence for hernia. Surgeons when implanting using on lay and inlay techniques will overlap the mesh 1.5 cm apart with sutures. These surgical techniques help allow for boundaries to compensate for any shrinkage that may occur.

2.2 Electrical Stimulation

2.2.1 Overview of Electrical Stimulation

Electrical stimulation has been used for decades to promote healing for a variety of wounds and even bone. Many current healing processes for wounds use a passive healing process by providing a healing environment and not necessarily engaging in advancing the healing process. Electrical signals relevance to wounds was discovered years ago and has been measured as the transepithelial potential (TEP) to be a DC current between 1 and 10 $\mu A/cm^2$ with an estimated current density of 300 $\mu A/cm^2$ [30].

Many research studies have explored how current can help cell migration to sites. The effect of frequency and type of current have also been explored with many studies in direct current and low frequency alternating current. In the 1950s studies were done with AC and were pulsed and promoted to be better at reaching nerve and muscle at greater depths. One study looked at the types of current used in clinical settings and the efficacy in laboratory settings and observed the effect frequency and signal type has in the outcome of electrical stimulation treatment. There are two types of alternating currents used the first being a pulsed current and the second being a burst modulated (BMAC). With pulsed being the earliest researched alternating current, but BMAC being more comfortable and better at strengthening muscle but with less understanding on reasons why it is more effective [31].

Alternating current being biphasic makes it more complex signal to understand and can be delivered in multiple ways. The signal can be delivered continuously, rectangular bursts, or modulated bursts. It is important to note the signal shape can be a sine wave or a rectangular alternating wave. The term modulated refers to controlling the amount of time the alternating signal is delivered [31]. The alternating signal has a set frequency and then within the bursts there is an additional frequency. In the case of this study the additional frequency is turning the ultrasound on for 15 seconds and then of for 15 seconds. For one minute the PZT disc will deliver a signal 50% of the time at a frequency of 610 kHz.

The frequency of the signal output is determined by the ultrasound and the specific disc type. The last type of alternating signal seen in clinical use is one that is used in the United Kingdom called Interferential Current (IC). The IC is generated by two independent alternating signals [31]. Two separate pairs of electrodes are used to deliver the two interfering AC signals. For these to work they are set at two different frequencies and are said to interfere within the tissue being treated. The study points out these uses do not take into account tissues that are nonhomogeneous and, for the purpose of nerve stimulation, their orientation [31]. For many applications this will not be effective because of the different impedances of muscle, fat, and connective tissues.

The application for the hernia repair mesh is experimenting with a high frequency alternating current. There is a vulnerable population of people that struggles with healing those who are diabetic or tobacco users. These individuals can hit a plateau in their healing process and the use of electrical stimulation can push them past this to heal faster and more fully. Studies have been done on external wounds to show that diabetic wounds can be characterized as lacking immune cells and extracellular matrix [32]. Kim et. al determine the effect of high voltage stimulation for use on diabetic rats by specifically looking at growth factors and collagen production [32]. The pulsed high voltage between 35-50 V for 40 minutes a day for 7 days starting with negative polarity followed by positive polarity resulted in enhanced healing. The enhanced healing caused by regulated levels of TGF-β_1, Collagen-1, and α-SMA. With TGF-β_1 importance on stimulating collagen deposition and angiogenesis [32]. The result showing the use of electrical stimulation to aid in diabetic model healing. The use of the modulating could be beneficial in achieving better tissue healing. Rouabhia et. al. discussed the importance of an electrical field signaling cells. In the case of hernia repair the goal is to enhance healing of the muscle of where the prosthetic is placed. Rouabhia et. al. examined the use of ES with fibroblasts. Fibroblasts are important in the healing process as they contribute to the tissue homeostasis. These cells regulated the turnover of the extracellular matrix (ECM) and are critical in helping injured tissues [30]. The study also confirmed electrical field generated by ES had no cytotoxic effects. A higher number of viable fibroblasts were seen

by the group exposed to the ES for 6 hours total than those not exposed. For this study they saw for their seeded heparin-bioactivated PPy/PPLA conductive membranes that there was a higher adhesion rate for fibroblasts exposed to the ES than those that were not [30]. If the EF is directing these cells for the purpose of this project the cells could adhere better to the mesh acting as the electrode compared to those that are not exposed to ES.

2.2.2 Electrical stimulation and electrodes

The type of electrode used in electrical stimulation is important in ensuring field delivery as well as being biocompatible. The synthetic hernia repair mesh is coated with gold sputter to become conductive on one side. Gold was chosen as it is bioinert and conductive. Many cellular studies examining electrical stimulation use gold interdigitated electrodes coupled with microfluidics for precision [33].

Future work on the project will examine the cellular interactions with the high frequency modulated alternating current.

2.3 Piezoelectricity

2.3.1 Piezoelectricity

Piezoelectric materials display properties that when under compression or in tension produce an electric charge. The two French scientists credited for discovering this effect are Pierre and Jacques Curie in the 1880s where they compressed different crystals and produced a voltage[34]. This effect comes down to their structure where when the internal molecules dipole moments get aligned from a strong electric field. When these dipoles are aligned a force applied in line with this axis will produce the electrical charge. Many piezoelectric materials today are artificially created and this process became popular in the 1960s [34]. One of these prevalent artificial piezo materials is lead zirconate titanate (PZT) and is what is used in this study. It is becoming more popular to use these materials as energy harvesters and sensors. An example of utilizing piezo materials as sensors could be in the case of using specifically

engineered piezo materials as a special sensor to be implanted in the body to collect mechanical biological parameters such as muscle tension. A piezo material can be fine-tuned and its parameters defined as charge constant, permittivity, elastic compliance, electromechanical coupling factor, and voltage constant [34]. For the purpose of ultrasound transducers that use a piezoelectric crystal to create the mechanical sound waves, the electromechanical coupling factor is how they measure the energy converted into acoustical waves. For the purpose of this study a readily available small PZT disc was used and the important factor was the poling direction. The poling direction, the mode, of a piezo material is the direction the dipoles are in, most often the poling direction is through thickness or radially poled. Through thickness is along the vertical axis of the material whereas radially poled is inwards and outwards from a circular object. This project uses a through thickness poled disc that will be compressed by mechanical ultrasound waves to produce an electrical charge.

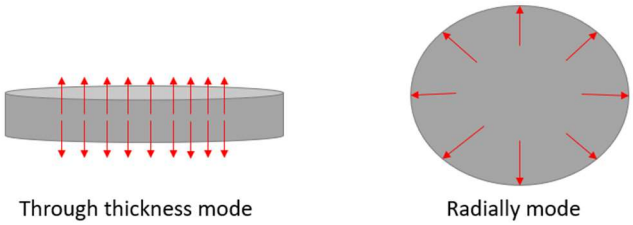

Figure 1 - Two Common Poling Directions (Modes) - Through thickness and Radial.

3.4 Ultrasound

3.4.1 Ultrasound Parameters

Ultrasound machines consists of high frequency sound waves by mechanically compressing air from a specially made transducer consisting of piezoelectric crystal. In the field of medicine ultrasound has a variety of applications from imaging diagnostics to therapeutic, and ablation. Clinical ultrasound is classified by the frequency and intensity. Diagnostic or imaging ultrasound is the highest frequency of 1-20 MHz, medium frequencies of 0.7-3 MHz is therapeutic, and low frequencies of 20-200 kHz are used in some clinical applications but mainly industrial purposes [35]. For imaging applications, the acoustic

impedance decreases at a higher frequency resulting in the use for imaging purposes to reach deeper tissues. These probes are also specially made to receive the backscatter to create and image from what the sound waves struck. It is important to understand how ultrasound waves travel through a medium and how they are affected by temperature, pressure, and medium type. As the wave travels from the probe into the object there will be attenuation. All these terms can be seen in Figure 2

Term	Definition
Attenuation	The decay rate of the ultrasound wave as it propagates through a medium.
Speed of Sound	How quickly the ultrasound wave is traveling through a medium. Most commonly units used are m/s².
Intensity	The power of the ultrasound wave exiting the surface of the ultrasound probe. Amount of power per surface area, i.e., 1.0 W/cm².

Figure 2 - Ultrasound parameters terms and definitions.

Attenuation is critical for the application at hand. If attenuation cannot be mimicked in the lab the power output generated could be significantly different from a real-world clinical application. Attenuation refers to the change in intensity and is frequency dependent it depends on the material type and the depth the wave travels. Given the same distance a higher frequency wave is attenuated more than a lower frequency wave A rule of thumb given for ultrasound through tissue is 0.5 dB/cm or each MHz of frequency [36]. The equation for attenuation can be seen in Equation 1. For human tissue the rule of thumb from McGarry et. al is 0.5 dB/cm per 1MHz of frequency. Given this. if there is 40mm of thickness and the ultrasound intensity at the face of the probe is 1.0 W/cm^2, then the intensity at the face of the disc would be 0.63 W/cm^2 using this calculation.

$$dB = 10 \log_{10} \frac{input\ intensity}{output\ intensity}$$

Equation 1 - Attenuation

$$Given: Attenuation\ 0.1\ then\ starting\ with\ 1.0\ W$$

$$0.1 = \log_{10}\left(\frac{1.0}{x}\right) \longrightarrow x = 0.79\ W$$

According to McGarry et. al there is a decrease in wavelength when the sound wave travels from soft tissue to fat tissue, it is slower in fat tissue [36]. When a structure compresses less than the kinetic energy of the wave will be absorbed less compared to a softer object.

3.4.2 Acoustic Properties of Tissue and Tissue Mimicking Materials

A material's ability to attenuate and ultrasound wave is called α and has been experimentally found for a variety of tissues. Several of these values can be found in Table 3. It is important to note that the attenuation for each tissue is different and for imaging purposes this determines what can be viewed along with the signal echoes received.

Table 3 - Acoustic Properties of Biological tissues

Tissue Type	Speed of Sound (m/s)	Density (kg/m^3)	Attenuation Coefficient (dB/cm) per 1 MHz
Soft Tissue	1575	1055	0.6-2.24
Soft Tissue Fatty	1465	985	0.4
Muscle	1547	1050	1.09

In addition, any time an acoustic wave strikes a boundary at an oblique angle there will be some form of reflection and refraction. The transition between the boundaries in tissue are not a consistent 90-degree transition if the fat is round over a section of muscle the ultrasound will be refracted according to Snell's law adapted from optics. Snell's law states, when the sound velocity in the second barrier is less than the first, the beam will propagate toward the center (Figure 2). Additionally, when the sound velocity in the second barrier is greater than the first, the beam will propagate outwards (away from the originating beam) in the latter condition most of the sound is reflected towards the transducer (Figure 3).

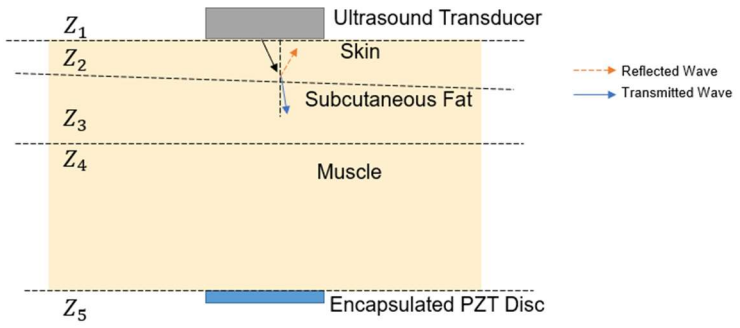

Figure 3 - Snell's Law of refraction and a schematic of ultrasound wave propagation through a composite medium.

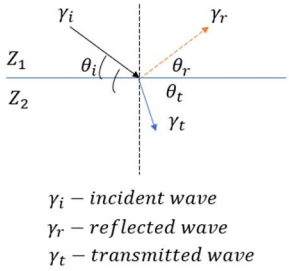

Figure 4 - Snell's Law diagram on refraction – Example above is when the beam is refracted toward the center because the speed of sound is less in the second barrier.

All the above acoustic parameters and understanding were applied when exploring different types of phantoms and why some might be better than others in mimicking specific tissues. Since many phantoms are a solid medium the objective is most often to match the overall attenuation, but it is difficult to match what might occur at the barriers throughout tissue.

2.5 References

1. Kulacoglu, H., *Current options in inguinal hernia repair in adult patients.* Hippokratia, 2011. **15**(3): p. 223-231.
2. Poulose, B., et al., *Epidemiology and cost of ventral hernia repair: making the case for hernia research.* The World Journal of Hernia and Abdominal Wall Surgery, 2012. **16**(2): p. 179-183.
3. Burger, J.W.A., et al., *Long-term follow-up of a randomized controlled trial of suture versus Mesh repair of incisional hernia. Discussion*. 2004, Hagerstown, MD: Lippincott: Hagerstown, MD. p. 578-585.
4. Langbach, O., et al., *Long-term quality of life and functionality after ventral hernia mesh repair.* Surg Endosc, 2016. **30**(11): p. 5023-5033.
5. Lange, B., et al., *Mesh penetration of the sigmoid colon following a transabdominal preperitoneal hernia repair.* Surg Endosc, 2003. **17**(1): p. 157-1.
6. Alters, M., *Determination of Clinical Efficacy of Ultrasound Stimulation on Piezoelectric Composites for Power Generation Applications*, E. Friis, C. Luchies, and L. D'Silva, Editors. 2019, University of Kansas.
7. Carmine Wang, S., K. Tiffany, and Z. Donghui, *Hernia Mesh and Hernia Repair: A Review.* Engineered Regeneration, 2020. **1**: p. 19-33.
8. O'Dwyer, P., et al., *Laparoscopic versus open repair of groin hernia: a randomised comparison.* Lancet, 1999. **354**(9174): p. 185-190.
9. Baylón, K., et al., *Past, Present and Future of Surgical Meshes: A Review.* Membranes, 2017. **7**(3).
10. Rognoni, C., et al., *Budget Impact Analysis of a Biosynthetic Mesh for Incisional Hernia Repair.* Clinical Therapeutics, 2018. **40**(11): p. 1830-1844.e4.
11. Ud-Din, S., et al., *Angiogenesis is induced and wound size is reduced by electrical stimulation in an acute wound healing model in human skin.* PloS one, 2015. **10**(4): p. e0124502-e0124502.
12. Bhang, S.H., et al., *Zinc Oxide Nanorod-Based Piezoelectric Dermal Patch for Wound Healing.* Advanced Functional Materials, 2017. **27**(1): p. n/a-n/a.
13. Sanders, D. and A. Kingsnorth, *From ancient to contemporary times: a concise history of incisional hernia repair.* The World Journal of Hernia and Abdominal Wall Surgery, 2012. **16**(1): p. 1-7.
14. Dowell, G., *A treatise on hernia: with a new process for its radical cure, and original contributions to operative surgery, and new surgical instruments. By Greensville Dowell*. 1876, Pennsylvania: Pennsylvania: D.G. Brinton, 1876.
15. Nyhus, L.M., et al., *The preperitoneal approach and prosthetic buttress repair for recurrent hernia. The evolution of a technique.* Annals of surgery, 1988. **208**(6): p. 733.
16. Usher, F.C. and S.A. Wallace, *Tissue Reaction to Plastics: A Comparison of Nylon, Orlon, Dacron, Teflon, and Marlex.* A.M.A. archives of surgery, 1958. **76**(6): p. 997-999.
17. Arnaud, J.-P. and P. Pessaux, *Surgical treatment of postoperative incisional hernias by intraperitioneal insertion of Dacron mesh and an aponeurotic graft.* Archives of Surgery, 1999. **134**(11): p. 1260-2.
18. Kingsnorth, A., *The management of incisional hernia.* Annals of The Royal College of Surgeons of England, 2006. **88**(3): p. 252-260.
19. Deerenberg, E., et al., *A systematic review of the surgical treatment of large incisional hernia.* The World Journal of Hernia and Abdominal Wall Surgery, 2015. **19**(1): p. 89-101.
20. La Mura, F., et al., *Emergency treatment of complicated incisional hernias: a case study.* Annals of surgical innovation and research, 2009. **3**(1): p. 15-15.

21. Den Hartog, D., et al., *Open surgical procedures for incisional hernias.* Cochrane Database Syst Rev., 2008(3).
22. Leblanc, K., *The critical technical aspects of laparoscopic repair of ventral and incisional hernias.* The American Surgeon, 2001. **67**(8): p. 809-12.
23. Pans, A., et al., *Long-term results of polyglactin mesh for the prevention of incisional hernias in obese patients.* World J.Surg., 1998. **22**(5): p. 479-483.
24. Trimbos, J.B., et al., *A Randomized Clinical Trial Comparing Two Methods of Fascia Closure Following Midline Laparotomy.* Archives of surgery (Chicago. 1960), 1992. **127**(10): p. 1232-1234.
25. Luijendijk, R.W., et al., *A comparison of suture repair with mesh repair for incisional hernia.* The New England journal of medicine, 2000. **343**(6): p. 392-398.
26. Raptis, D.A., et al., *A Comparison of Woven Versus Nonwoven Polypropylene (PP) and Expanded Versus Condensed Polytetrafluoroethylene (PTFE) on Their Intraperitoneal Incorporation and Adhesion Formation.* The Journal of surgical research, 2011. **169**(1): p. 1-6.
27. Greca, F., et al., *The influence of porosity on the integration histology of two polypropylene meshes for the treatment of abdominal wall defects in dogs.* The World Journal of Hernia and Abdominal Wall Surgery, 2008. **12**(1): p. 45-49.
28. Orenstein, S.B., et al., *Comparative Analysis of Histopathologic Effects of Synthetic Meshes Based on Material, Weight, and Pore Size in Mice.* The Journal of surgical research, 2012. **176**(2): p. 423-429.
29. Lee, L.H., *Randomized clinical trial of groin hernia repair with titanium-coated lightweight mesh compared with standard polypropylene mesh (Br J Surg 2008 95: 1226–1231.* British Journal of Surgery, 2009. **96**(2): p. 221-221.
30. Rouabhia, M., et al., *Electrical stimulation promotes wound healing by enhancing dermal fibroblast activity and promoting myofibroblast transdifferentiation.* PloS one, 2013. **8**(8): p. e71660.
31. Ward, A., *Electrical Stimulation Using Kilohertz-Frequency Alternating Current.* Phys. Ther., 2009. **89**(2): p. 181-190.
32. Kim, T.H., H.-y. Cho, and S.M. Lee, *High-Voltage Pulsed Current Stimulation Enhances Wound Healing in Diabetic Rats by Restoring the Expression of Collagen, α-Smooth Muscle Actin, and TGF-β1.* The Tohoku Journal of Experimental Medicine, 2014. **234**(1): p. 1-6.
33. Koh, K., *Effects of alternating current electrical stimulation on the cellular chemistry and proliferation of C2C12 muscle cells*, D. Nawarathna, D. Ewert, and T. Gustad, Editors. 2016, ProQuest Dissertations Publishing.
34. APC International, L., *Piezoelectric Ceramics: Principles and Applications.* APC International., 2011.
35. Ahmadi, F., et al., *Bio-effects and safety of low-intensity, low-frequency ultrasonic exposure.* Progress in biophysics and molecular biology, 2012. **108**(3): p. 119-138.
36. McGarry, C.K., et al., *Tissue mimicking materials for imaging and therapy phantoms: a review.* Physics in medicine and biology, 2020.

Chapter 3: Journal Article

This section contains a manuscript to be submitted for publication with the Journal of Medical Devices

Determination of a Clinically Relevant Tissue Phantom for Transcutaneous Ultrasound Stimulation of Piezoelectric Discs for Current Density Applications

Authors:

Anna Norman
Spine Biomechanics Laboratory,
Department of Bioengineering,
University of Kansas,
Lawrence, KS 66045
Email: anna.norman@ku.edu

Luke Lindemann
Spine Biomechanics Laboratory,
Department of Bioengineering,
University of Kansas,
Lawrence, KS 66045
Email: lindemanluke@ku.edu

Morgan Riley
Spine Biomechanics Laboratory,
Department of Bioengineering,
University of Kansas,
Lawrence, KS 66045
Email: morgan.riley@ku.edu

Victoria Drapal
Spine Biomechanics Laboratory,
Department of Bioengineering,
University of Kansas,
Lawrence, KS 66045
Email: Victoria.drapal@ku.edu

Dr. Jennifer Robinson
Professor,
Department of Chemical and Petroleum Engineering
University of Kansas,
Lawrence, KS 66045
Email: jlobinson@ku.edu

Elizabeth Friis*
Professor,
Department of Mechanical Engineering,

University of Kansas,
Lawrence, KS 66045
Email: lfriis@ku.edu
* Corresponding Author

3.1 Abstract

The most common abdominal surgery is a hernia repair surgery [7]. A hernia can be caused for a variety of reasons and is seen across all demographics [7]. There could be underlying health conditions that are cause for a weakened muscle that lead to a protrusion or breakthrough the abdominal muscle or groin. However, it can also occur from trauma and in some case no known reason. For being such as common surgery that is performed every year there are still little advancements in technology to increase healing rates and reduce infection and recurrence rates. The use of electrical stimulation has been proven to improve healing process of wounds and could benefit soft tissues like muscles as well [12]. This includes the use of an alternating current signal [12]. Piezoelectric materials have been shown to be good sources of electrical charge especially in cases where a battery pack is inconvenient and the size needs to be small [37]. To stimulate a piezoelectric material for use as a transcutaneous implant, ultrasound has proven to be successful in providing necessary mechanical loading for current density generation. Ultrasound has been shown to be able to sufficiently load lead zirconate titanate (PZT) discs to produce voltage [6]. However, there is no research in the best phantoms for benchtop testing of implanted devices that require ultrasound stimulation. In order to determine which tissue phantoms are good candidates for this testing different types were created and their effect on power and voltage output of the PZT compared to that of a porcine tissue sample. Parameters that were examined were reusability, power output, and voltage output. The study of different ultrasound phantoms (N=5) for each 5 groups was performed to compare a single disc output in a resistance sweep. The groups being: Unflavored edible gelatin (Kroger® gelatin), unflavored edible gelatin + sugar free Metamucil®, Humimic® Gelatin #0 (Gelatin #0), Humimic® Gelatin #0 with added sugar-free Metamucil®, and the porcine tissue control consisting of skin, fat, and muscle. The root-mean square voltage output for each group of phantoms with ultrasound intensity of 1.0 W/cm^2 was compared along with the power generation of a single PZT disc. The goal was to determine which phantom was the best to be used in mimicking porcine skin, fat, and tissue in the application of transcutaneous electrical stimulation with PZT generators. A sub study of the resistance sweep was used to determine the voltage output and thus current density to be provided to a hernia repair

mesh with a range of areas. The results of this study show an appropriate phantom with long term stability to best mimic transcutaneous replication for an embedded piezoelectric power source is gelatin #0 or gelatin #0 with Metamucil®.

3.2 Introduction

Every year hernia surgeries in the U.S. exceed 1 million according to the Food and Drug Administration (FDA). A hernia occurs when there is protrusion through the abdominal wall most commonly this is seen with the intestines. A hernia can occur in any demographic. Historically in the 1900s hernias were repaired with suture techniques performed by skilled surgeons. However, nowadays to better mitigate hernia recurrence a prosthetic implant of synthetic mesh is used. This mesh acts as a "net" like structure to strengthen the weakened abdominal wall. It has been shown the mesh is reduces national recurrence rates below 5% [7]. However, with the use of a mesh there are additional complications that often occur: inflammation, chronic pain, adhesion, and infection. Many times, the healing process is affected by the body's inflammatory response which can impact a lack of tissue integration into the mesh. If electrical stimulation has been shown to better direct cells to wound sites then introducing this to the mesh could aid in better and faster healing for patients [11]. This research study focuses on whether a single piezoelectric disc can generate sufficient current for the needed current density for enhanced healing and what material is best to mimic the abdominal tissue. The main goal compared the effect of tissue phantom type on the average power output and root mean square voltage output for the PZT to that of the porcine tissue. Each of the phantoms will have different acoustic properties such as speed of sound and attenuation and this will directly affect the mechanical loading of the PZT. It is important for the tissue phantom to be similar in these outputs to that of porcine tissue as that is the control for the study. This study determined the most clinically relevant tissue mimicking phantom that is readily accessible to be used with the therapeutic ultrasound to mechanically stimulate the single disc.

3.2.1 Piezoelectric Materials

Energy harvesting low frequency

A new area of research and applications has emerged in the field of energy harvesting. Particularly harnessing the special characteristics of piezoelectrical materials to harvest energy from mechanical vibrations. Many of these applications however use a low input frequency [38]. The ability of piezoelectric material to be placed in a sensor or small device is advantageous as many of these small electronic devices only need mW to μW of power output. Specific piezoelectric material, resonant frequency, size, and capacitance rating can be chosen to regulate the desired output of the PZT [38]. One reason piezoelectric material is more efficient than other methods of transforming mechanical energy such as electromagnetic or electrostatic induction is because the piezoelectric materials provide a higher energy density and are more versatile with a variety of systems. The crystalline structure of a piezoelectric materials with non-overlapping positive and negative charges yields a dipole moment. When these crystalline structures are compressed by mechanical loading these dipoles become distorted producing an electrical charge. In addition, there two different common modes of poling for piezoelectric discs. The first being through thickness poled where the compression on the vertical axis produces the charge. The next being that of radially poled where the poling direction is radially on a circular disc like material. The radially poled are more forgiving in the angle of incident of the mechanically provided load. For higher frequency applications the choice of piezoelectric materials is simple in that most often it is chosen for the highest power output at the materials resonant frequency [38]. An application of using piezoelectric discs placed in stacks with compliant layers showed there was a decrease in impedance and an increase in power generation when stacked with compliant layers [39]. The increase in power generation and lower impedance is important for the spinal fusion implant explored by Goetzinger et. al. for promotion of bone growth through DC stimulation. An even more recent study performed by Krech et. al. showed the effect of uniform thin epoxy layers in between discs increased the power generation and by connecting discs in parallel the impedance was lowered [37]. However, for the purpose of soft tissue

healing there have been studies showing even low levels of alternating current have produced enhanced healing [12]. Suggesting even a single disc can create the necessary output for the application.

The idea of using two discs electrically in parallel yet connected in the same plane to remain flexible was explored, however a single disc produced enough voltage and current for the given surface area of hernia mesh. A limitation for soft tissue is the range of sizes and for a hernia repair application that uses laparoscopic surgery it needed to be small enough to fit in a cannula and a smaller size means more comfortable for patients' post-surgery. However, future applications could use two discs or more to create a greater chance of striking the disc with ultrasound.

The difference between previous focus on a piezoelectric material used on an implant for bone is that uses a frequency of human walking because it is stimulated through physiological loading. In the case of hernia repair mesh this study used ultrasound to stimulate. Medically safe therapeutic ultrasound is readily available and been shown to be effective in stimulating PZT discs [6, 40]. Ultrasound is characterized by three main parameters: frequency, intensity, and cycles. The level of frequency of a ultrasound corresponds the penetration depth with lower frequencies penetrating deeper less than or equal to 1MHz as compared to imaging ultrasound 1-20 MHz [35]. However, the higher the frequency the shorter the wavelength and the shorter wavelengths attenuate faster. The intensity corresponds to the amount of energy transferred with therapeutic ranging from 0.1-3.0 W/cm^2. The intensity of ultrasound will be directly related to how much power is generated by the PZT. The duty cycle refers to how much the ultrasound is "on" during a cycle. For this study the cycle is a continuous duty cycle for the time it is on it is all on. For example, if it was 50% duty cycle and it was on for 30 seconds then the wave will be only generated for a total of 15 seconds.

3.2.2 Tissue Mimicking Phantoms

When using ultrasound in a laboratory setting it is important to use an appropriate medium for the waves to travel through. In this case, the goal was to investigate whether a single disc could provide

enough output for the given area of a hernia repair mesh to meet current density needs and determine the best type of tissue phantom to use for this application. For a comparison cuts from pork loin in the Longissimus muscle were purchased from a butcher and used with skin, fat, and muscle intact. One study by Koch et. al examined ultrasound data on porcine because many times in the meat industry this is used to quantify fat content of a cut of porcine [41, 42]. For the muscle of the porcine they saw an attenuation at 1.0-1.2 dB/MHz compared to the attenuation of skin and backfat of 1.6-2.7 dB/MHz [41, 42]. For skin only they saw an attenuation of 0.7 dB/MHz; this differed from previous studies in the literature of 7-13 MHz at 25 °C but difference in region, breed, and age play an important role in the collagen in the porcine skin [41, 42]. The study also notes that the greatest transition boundary for the speed of sound of the ultrasound occurs the skin-fat boundary and is because the speed of sound is significantly greater in skin than in backfat layers [42]. In addition, the amount of poly unsaturated fatty acids in the subcutaneous layer showed a significant influence on the sound velocity. This was not something was measured for this study, but the thickness of fats was measured and kept relatively the same for each specimen and the skin thickness was the same across all specimens. All porcine specimens were tested at room temperature as compared to some studies that use hot carcasses for the meat industry. To create relevant tissue phantoms with clinically relevant attenuation all manufactured specimens were compared to the porcine specimens.

There are a variety of different ultrasound phantoms commercially available and research recipes for in-house creation. The study at hand examines a commercially available phantom to mimic soft-fatty tissue: Gelatin #0 from Humimic®, Gelatin #0 with sugar-free Metamucil®, unflavored store-bought gelatin powder, unflavored store-bought gelatin powder with sugar free Metamucil®. The brand name sugar-free Metamucil®, sugar-free psyllium hydrophilic mucilloid fiber was used to increase the amount of echo for the ultrasound. This is often used in imaging ultrasound phantoms for training [36]. All of these were of equivalent height ±2mm and roughly same volume of pork loin with skin still on. It was hypothesized that the impact of skin and having actual boundaries of tissue would result in a lower power

generation from the disc, and that the phantoms with mix ins would result in more attenuation than those without. This increase in attenuation will result in lower mechanically loading of the disc and thus power output. Attenuation encompasses, scattering, reflection, and absorption. Materials with mixed in particles will have more of all three of those characteristics. It was important to test all specimens at room temperature because if the specimen was too cold through the mediums center it can affect the propagation speed and attenuation [43]. For colder specimens the propagation speed decreases, but attenuation was more stable for a smaller range of temperatures. In addition to tissue phantom evaluations, an estimation of hernia repair mesh surface area for the electrode was made and a resistance sweep performed to create a circuit to deliver the proper current density to the sputter coated mesh.

3.3 Methods

3.3.1 Circuit Identification

The goal of the circuit is to deliver the voltage created by the piezoelectric to the mesh. For testing purposes to determine how the power generation is across various resistances a shunting resistance sweep was used 30 -1510Ω. The use of capacitor was explored but deemed not necessary for proof of concept of this project. By using the shunting resistance sweep which has been used with PZT in the past this allowed the peak power to be seen and the ability to see voltage drop across larger resistances. A cable with a 10Ω resistor in it was used to measure the voltage drop across. This cable is in parallel with the 1 MΩ resistor input of the channel of the oscilloscope. A TEKTRONIX Mixed Domain Oscilloscope with 2.5 GS/s sample rate, MDO3012 was used for electrical signal collection. A schematic of the oscilloscope and circuit connection can be seen in Figure 5. A resistance box was used to vary the resistances. The results from average power produced by the PZT can be plotted versus total resistance to see the peak power of the PZT for the given frequency and intensity of ultrasound loading.

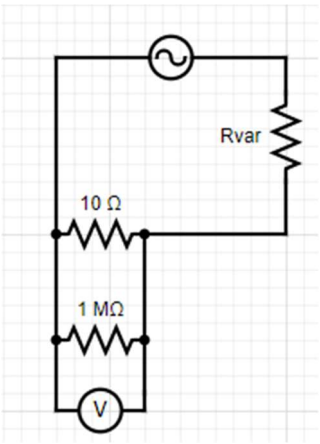

Figure 5 - Circuit with the voltmeter acting as the oscilloscope with the input channel of 1 megaohm resistance in parallel with the cable.

3.3.2 Disc Identification

A piezoelectric disc (STEMiNC, Doral, FL), modified PZT-4 (SMD7T04S111), with a diameter of 7 mm and thickness of 0.4 mm. This specific lead-zirconate titanate disc is through thickness poled and is of the hard material type of PZT. It was chosen based on availability and preliminary tests showed sufficient power generation.

An 8.5 cm diameter Falcon petri dish was used as the base for the PZT disc. Using silver conductive epoxy, EPO-TEK H20E conductive epoxy (Epoxy Technology, Billerica, MA),, the thin wires were adhered to the disc on both sides and cured in the oven for 30 minutes at 130 °C. Liquid electrical tape was used on the wires from the disc base leaving 1.5-2 cm of exposed wire for clipping. This disc was then checked for electrical connection and adhered to petri dish using rubber cement. Following adhering silicone (Dragon Skin, Smooth-On Macungie, PA) to encapsulate disc and partial wires to protect from elements. The silicone was not medical grade as all studies with this disc will be outside of cell well plates. Future work and products will use medical grade silicone.

3.3.3 Tissue Mimicking Phantoms

Determining the types of tissue phantoms was key in trying to best mimic tissue. For a control 5 porcine specimens were chosen. The pork tissue samples came from loin of the pig and consisted of layers of skin, subcutaneous fat, and muscle. They were carefully cut to size to fit within the petri dish over the encapsulated disc. All tissue samples were 40 mm tall when relaxed and the layers of skin, subcutaneous fat, and muscle were measured and recorded respectively Figure 3. Total heights were the same but given the limitations of the porcine specimens there was some variability in thickness of fat and muscle. For testing purposes, a rigid taper cylindrical support structure with a large diameter of eight cm and small diameter of six cm was placed around the tissues on the petri dish to providing a boundary. The taper cylindrical support structure was needed to act as a grounding barrier for the tissue sample in order to prevent sheering at the layers.

3.3.4 Phantom Material Thickness Determination

A hernia can occur for anyone in the population and across a wide range of abdominal wall thicknesses. In choosing an abdominal wall thickness the ultrasound may need to propagate through a study was examined that had a range of patient's BMI from <30 and >50. Many surgeons will not operate when a BMI is above 40 or strongly recommend against it. Surgeons speculate less complications are present when BMI is less than 30 for operation. For a study performed in 2016 by General Surgery News the average BMI for patients was just under 35 kg/m^2. The purpose of the study was to examine surgical site infections, surgical site events, and recurrence. They found no correlation between recurrence and patient BMI. With the knowledge of a wide range of BMI of patients a BMI of 28 was chosen, slightly above the average adult population and this was used in conjunction with the BMI and abdominal wall thickness data paper to determine an estimate for abdominal wall thickness. It was determine this corresponded to 40 mm [44]. Specimens of 39 mm ± 1mm were used. The study for individual characteristic abdominal wall thickness measured the thickness of muscle and fat as those were the main contributors to the thickness. For this study similar percentages of composition of fat and muscle was chosen for the porcine tissues. A schematic depicting this can be seen in Figure 6 below.

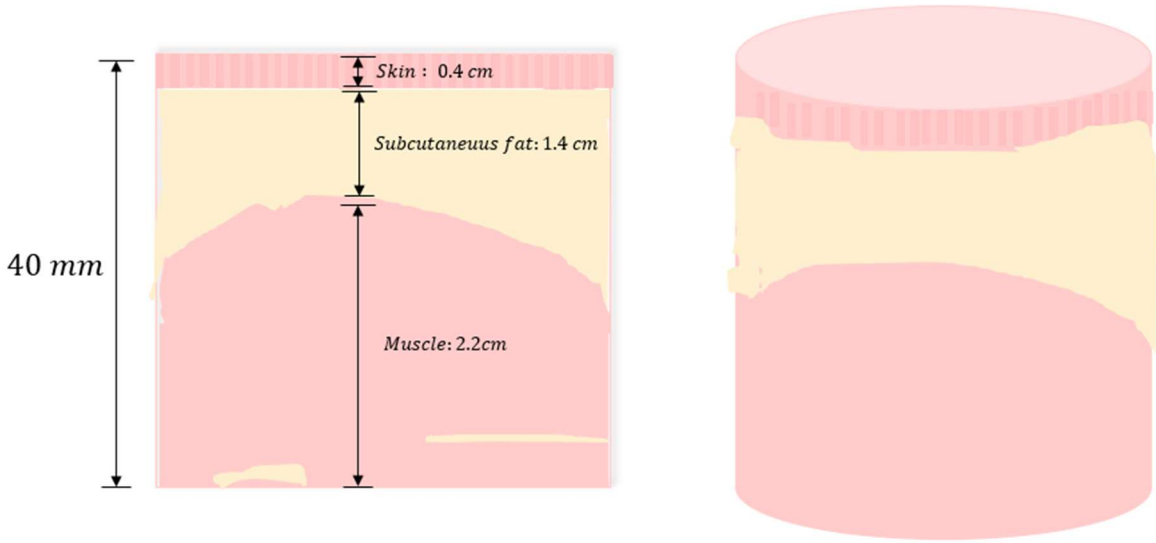

Figure 6 - Section View of Porcine Specimens.

Figure 7 - Porcine Tissue Sample with all Skin-Fat-Muscle Boundaries intact post slicing.

Gelatin #0 Humimic® Manufacturing Medical Ultrasound Phantoms

Gelatin #0 (Humimic®, manufacturer name, item number or other identifier, and company location) was chosen as it is manufactured to match the acoustic properties of soft fatty tissue. The values for soft tissue, soft tissue fat, and muscle can be seen in Table 1. The values for Gelatin #0 can be seen in Table 2. It is noted that the attenuation for the gelatin #0 is closest to the soft tissue fatty values with a

low attenuation. It was hypothesized this will result in a higher power output seen for the gelatin 0 specimens as this phantom has the lowest attenuation. The attenuation of ultrasound is frequency independent and is only affected by the depth and the material type of the medium. These gelatin specimens were created by melting the gelatin at 130 °C (266 °F) for 4 hours in the oven per manufacture instructions.

Figure 8 - Gelatin #0 from Humimic, 40 mm thick through the center

Table 4 – Acoustics Parameters for Biological Tissues

Tissue Type	Speed of Sound (m/s)	Density (kg/m^3)	Attenuation Coefficient (dB/cm) per 1 MHz
Soft Tissue	1575	1055	0.6-2.24
Soft Tissue Fatty	1465	985	0.4
Muscle	1547	1050	1.09

Table 5 - Acoustic Parameters for Crafted Tissue Phantoms

Tissue Phantom	Speed of Sound (m/s)	Density (kg/m^3)	Attenuation Coefficient (dB/cm) per 1 MHz
Agar Based	1544 +/- 3.1	1050	0.5 @ 3 MHz
Gelatin (water based)	1520-1650	1050	0.12-1.5
Humimic® Gelatin #0	1449.30	880.379	0.223 +/- 0.002

Edible Gelatin

The generic edible gelatin was the same recipe as seen in Alters et. al. with a ratio of approximately 10:1 water to gelatin, mL of water to g of gelatin. Gelatin has been an easy tissue mimicking phantom as it is readily available and can be controlled based on the ratios of gelatin and water mixed up. This phantom is expected to provide more attenuation than that of the Gelatin #0. Alters et. al. cites the gelatin and plastic wrap combination to mimic skin and tissue [6]. The mixture is then cooled in the fridge for up to 2 hours and tested No samples were allowed more than 24 hours before testing as the gelatin can begin to degrade and is not stable to be left at room temperature for a long period of time. The edible gelatin mold had to remain in the silicone mold in order to maintain its integrity, so the orientation of this mold for both this and edible gelatin + Metamucil® was the slightly smaller diameter on the bottom over the disc (upright position) and did not have the styrofoam cup as it was in the silicone mold. It is not expected this geometry affected the ultrasound as the height was the same and the ultrasound probe face was still smaller than the base diameter. The volume was the same as that used in Gelatin #0 and all Metamucil® samples.

Metamucil® Samples

From literature people have tried to incorporated mix-ins to help better mimic backscattering for imaging purposes and better estimate attenuation by providing elements that make the material more complex [36]. One such readily available mix-ins is sugar-free Metamucil®. The small particulates provide backscatter which for imaging purposes is important to practice with to find a clear image of an organ. For the purposes of this study it helped provide more realistic attenuation. It was expected the samples with the Metamucil® would provide dampening effect to the ultrasound waves. The recipe was the same as the edible gelatin but 17.6 g of Metamucil® added. The water content was not equal for the edible gelatin samples and the Gelatin #0 specimens, so the edible gelatin-Metamucil® sample was determined first and the Gelatin 0# amount Metamucil® cut by half.

The Metamucil® for the edible gelatin specimen was mixed in following the 10 minutes mixing of gelatin powder and carefully avoided any clumps and cooled for 30 minutes and poured into the mold

the same way as the edible gelatin. For the Gelatin #0 mold following the 3-4 hours of melting the Metamucil® was carefully mixed in and all clumps taken care of and placed in the oven for another 3 hours. Detailed methods can be seen in Appendix B.

Figure 9 – Edible Gelatin with Metamucil® in Mold with Plastic Wrap on top.

3.3.5 Ultrasound Testing

Ultrasound testing was performed using the Chattanooga Intelect TranSport machine. The frequency was set to 1 MHz a continuous duty cycle and intensity set to the max for this study of 1.0 W/cm^2. The petri dish with the disc was placed on a piece of delrin that a thin textured silicone piece to help prevent sliding with a total height of X from the tabletop. The disc was then electrically connected to the resistance sweep circuit. The face of the ultrasound transducer was fixed using a vice and kept in contact parallel to the phantom surface by blue 3M tape to keep the probe from sliding upwards.

Figure 10 - Disc on petri dish with pork tissue compressed ontop of coupling gel and disc to ensure a good boundary.

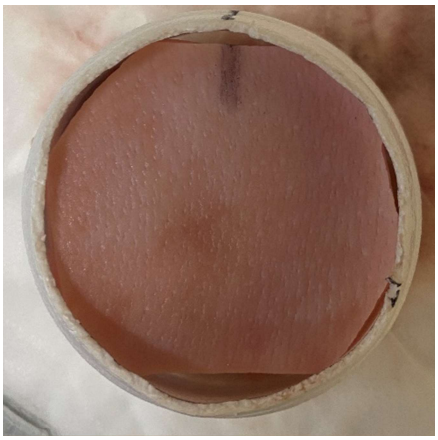

Figure 1 - Top view of pork specimen line indicates alignmint with the petri dish and the styrofoam cup for consistency between runs.

Figure 12 - Ultrasound Testing setup with probe fixed in vice and tape holding the transudcer face from rising up during testing by providing slight pressure.

Minimal pressure was applied with the tape to keep from applying abnormal pressure to the phantom. The goal was the keep the transducer in contact with the surface of the phantom to best mimic a clinical setting. The ultrasound was then turned on and disc and transducer repositioned to find the maximum output from the oscilloscope. The resistance sweep starting with a resistance on the box set to 20 ohms then begins with 15 seconds on and then 15 seconds off up to the 1510 ohm. With a total amount of time on equal to 4.5 minutes. This amount of time is safe for therapeutic ultrasound [45]. Following completion, the ultrasound is turned off and disc checked on the impedance capacitance resistance machine (LCR) to ensure connection is maintained and encapsulation is intact and 15 minutes to allow disc to "cool off." For each specimen 6 runs were performed and then averaged for that specimen. Any run where the probe slips or data points are not saved are left out and an additional run performed these are noted in lab notebook and raw data notes.

The porcine specimens could reach room temperature and measured using a thermocouple before the start of run. To preserve them they were placed in the refrigerator for the 15 minutes in between runs as was the edible gelatin specimens as they are not stable at room temperature for a long period of time. Once finished with testing the porcine tissues were wrapped in saline towels and placed in the freezer and

the number of times thawed and frozen written down. A test run was performed with a “cold” sample below 70 degrees and this provided a smaller output which corresponds to a lower speed of sound in lower temperatures [46].

For the edible gelatin specimens, the plastic wrap acted as a barrier for the probe and coupling gel as coupling gel is water soluble and would create air bubbles if in direct contact with the edible gelatin specimens. Additionally, in preliminary studies when the disc became warm and there was a long period of time of the coupling gel in a slightly warmer environment with the gelatin #0 small inclusions would begin to form in the gelatin #0. To combat this a thermocouple was used for 6 runs and saw no measurable increase and the cooling of 15 minutes in between was introduced.

3.3.6 Hernia Repair Mesh

Polypropylene mesh is for the in vitro cellular testing with the piezoelectric single disc generator. The type of mesh used is PPKM505 0.125 mm monofilament 1.3 x 1.5 mm pores 58 GSM from Surgical Mesh™ Division Textile Development Associates, Inc. This mesh was chosen because of the larger pore size and light weight.

3.3.7 Sputter Coating

The hernia repair mesh sputter coated with 99.999% gold to a thickness of 100 nm The role of sputter coating allows for precise placement of atoms to a substrate which is extremely useful for medical implants.

3.3.8 Surface Area Estimation for Hernia Repair Mesh Application

The surface area of the sputter coated mesh was estimated three different ways. The surface area is critical in the application because it is a factor in the current density calculation. The current across the surface area of the electrode determines the current density output. The first estimation was by hand and detailed methods involving the filament’s diameter and knitting-woven pattern. The lengths of the

filaments were measured, and top curved surface area was used excluding top and bottom faces and treated as a portion of a cylinder using the known filament diameter. Following the knitted-woven pattern and measurements a surface area was estimated.

The next method of estimation used was taking a picture using the microscope and then using ImageJ to count the number of gold pixels per that unit area to determine the porosity percentage.

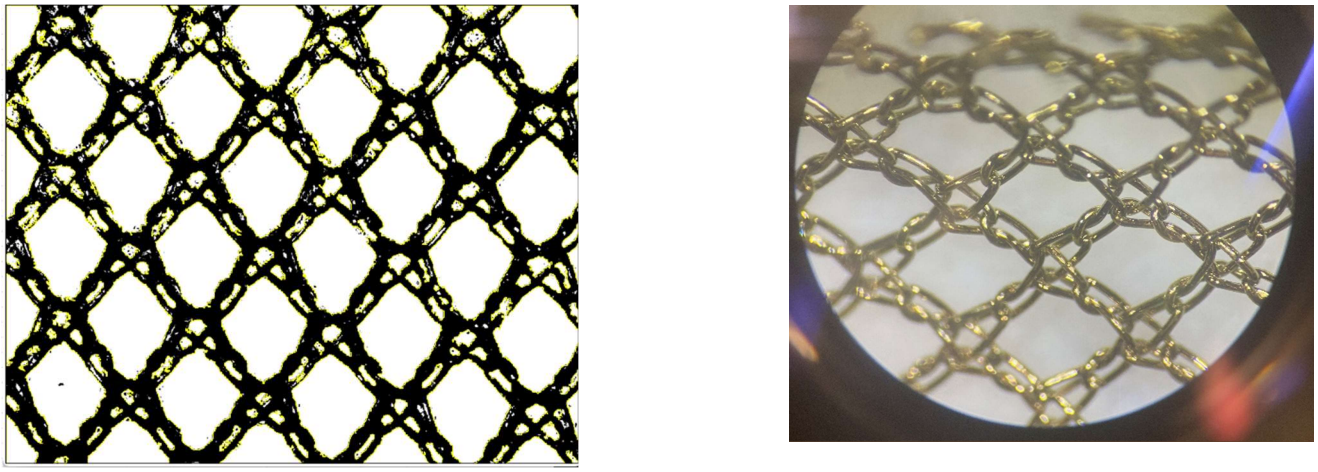

Figure 13 - ImageJ picture of mesh the highlighted portions are for the white space within the pores. The porosity can be found by using the white area divided by the total image area.

Lastly, a research paper examined the porosity of prosthetic meshes. Similar to hernia repair meshes there are a variety of types of prosthetic meshes used in cardiovascular implants, namely vascular prosthetics [47]. This paper used two different methods the first being weight and the next being area using topographical imaging. The area method was more precise and could be used for all mesh types. A similar type of mesh was used in this study, given their range of pore sizes and same knitting pattern the estimation is given in the table.

Table 6 - The porosity estimations. These can be used to determine the estimated surface area. Since the estimated measured surface area was close to the porosity from the paper with similar pattern this was used for the surface area calculations.

	Paper Estimation	Measured and Calculated Estimation	ImageJ Estimation
Porosity	60.10%	55.70%	40.00%

The assumed total area to be used in the future cell study was estimated to be 19.93 cm^2 using the manual calculation method.

3.3.9 Data and Statistical Analysis

Voltage data was obtained using the oscilloscope across the 10-ohm resistor. For comparison across the different types of phantoms the average power for was taken for each resistance across the entire resistance sweep. This allowed the curve for the PZT to be found across the varying resistances. The PZT should peak at the same specific resistance across the different phantoms. Mathworks (Nitwick, MA) MATLAB code was adapted from Alters et al. [6]. The files from the oscilloscope were saved as .csv (comma delimited) files and file path read in from MATLAB. The adapted code utilized a Butterworth filter of the 5^{th} order with cutoff frequency of 1.2 MHz in order to filter any noise out. The data files had a sample collection of 100 Ms/s with 10,000 points collected. The raw voltage data post filtering was used to calculate the root mean square voltage using equation two. Using the Vrms and the total resistance of the circuit the power output from the single PZT disc could be found. The equation for power can be seen in equation three.

$$V_{rms} = \frac{V_p}{\sqrt{2}} \tag{2}$$

Equation 2 - Root Mean Square of Voltage

$$P = \frac{V_{rms}^2}{R} \tag{3}$$

Equation 3 - Instantaneous power for a given circuit element.

However, for the purpose of the hernia repair mesh the interest was in current density. To determine this the voltage, drop across the resistor was taken as it will be in parallel with the mesh acting as the electrode so the voltage will be the same across them. This root mean square voltage is then used with the resistance that could be seen by the soft tissue muscle. In the cellular studies they can measure the resistance of the solution and that can be used with the current in order to determine the actual current density from the given output voltage. Given the resistances measured and seen in literature for muscle were found to be 750-1000 Ω and for fat it is 1000-5000 Ω [48]. If in contact with muscle assuming a 1 kΩ resistance the current density would be calculated as follows.

$$Ohm's\ Law\ I = \frac{V}{R} \tag{4}$$

Equation 4 - Ohm's Law used to calculated current through a given resistance

The average power and root mean square voltage for the 6 runs of each specimen with 5 specimens of each type of phantom were found and plotted accordingly. The mean for all 5 specimens for each group was found along with the standard deviation both for power and root mean square voltage. The mean voltages for groups of phantoms across the resistance sweep was used to determine current density delivered to the 6 well plates for the cellular study. Following data analysis, a one-way analysis of variance (ANOVA) was used to determine significant difference in power production across the different types of phantoms. Furthermore, a Tukey-Kramer *post hoc* analysis was used to determine a statistically significant difference among the different groups of phantoms using an α=0.05.

3.4 Results

3.4.1 Effect of Phantom Type on Power Output

Each group of phantoms had 5 specimens in them (n=5) aside from one porcine specimen was 35 mm instead of 39 ± in height. This specimen was not included in the study. Each specimen had 6 runs across the resistance sweep and all 6 runs were average for that one specimen and then all 5 specimens

values averaged for that group. Giving each type of phantom 30 runs with 5 different specimens for a total of 25 specimens and 150 resistance sweep runs. Figure 11 shows the average power the PZT produced when each type of phantom was used.

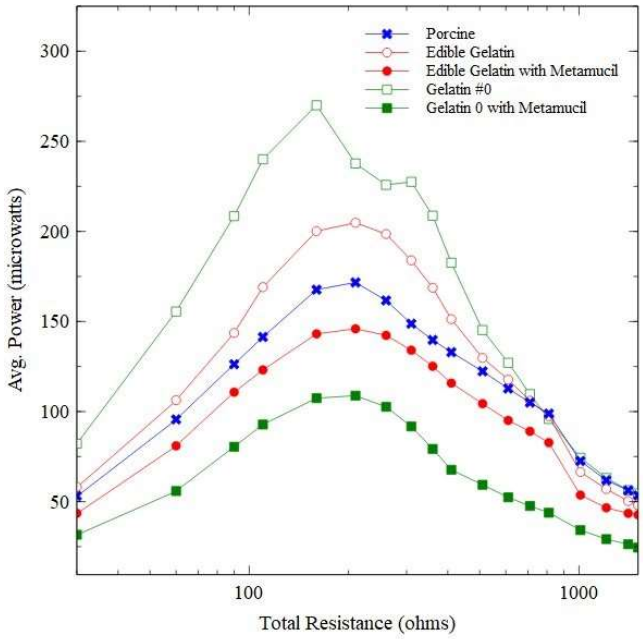

Figure 14 - Average Power of all 5 specimens in each group of phantoms plotted versus the total resistance. Note the resistance is on a log scale.

The average maximum power produced by the PZT was compared across each type of phantom. There was no statistical difference between each type of phantom and the porcine tissue.

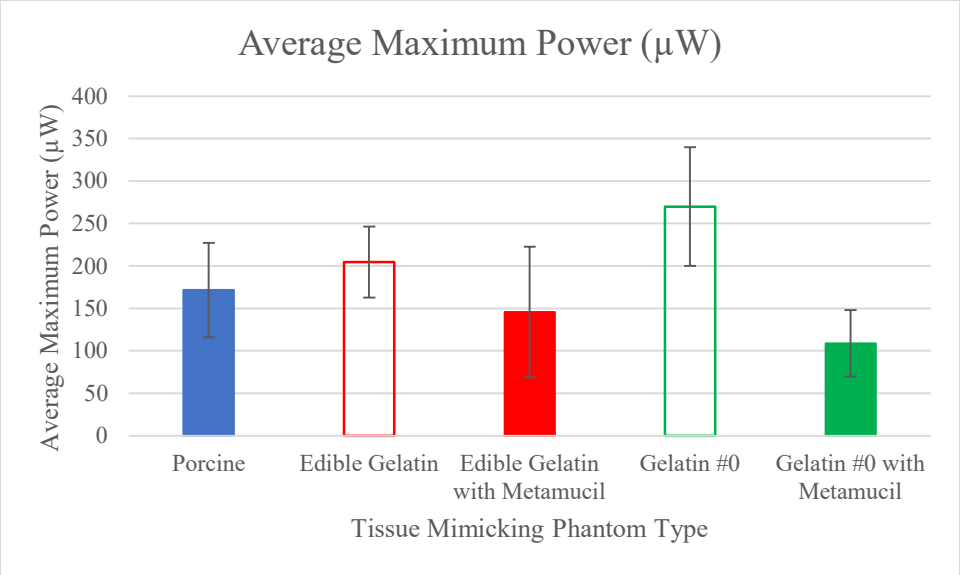

Figure 15 - Average Maximum Power Produced by PZT by each group.

The average power at one kiloohm was compared for each phantom type to the porcine using the Tukey-Kramer test alpha equal to 0.05. The gelatin #0 with the fiber additive was found to be statistically significant at this resistance. The fiber additive gelatin #0 was statistically significant with a lower power output at 1 kiloohm of resistance. The comparison can be seen in Figure 13.

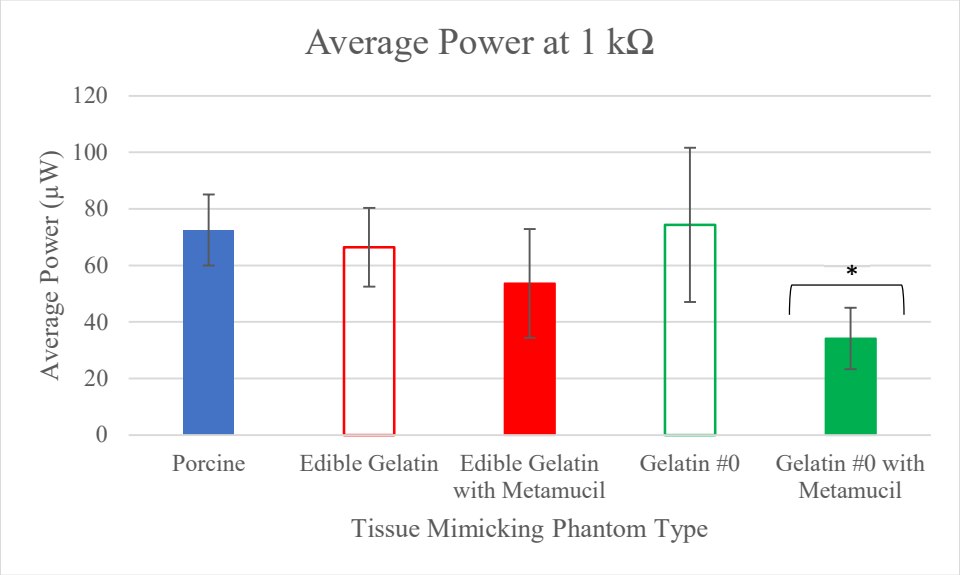

*Figure 26 - Average Power Produced by PZT by each group. * indicates statistically significance alpha equals 0.05.*

3.4.2 Effect of Phantom Type on Voltage Output

Each phantom was tested with the PZT and the root mean square voltage outputs plotted in Figure 14. The signal was not transformed from an AC signal, but for comparison purposes the root mean square (Vrms) of the voltage drop was calculated from the raw voltage.

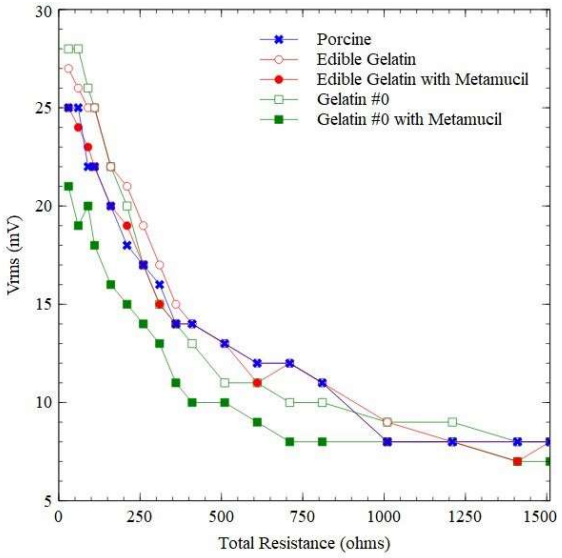

Figure 17 - Vrms vs. Total Resistance for the average across the 5 specimens in each group of phantoms. Note the resistance is on a log scale.

The average maximum voltage for each phantom type was compared to porcine using the Tukey-Kramer test. The gelatin #0 with Metamucil® was statistically significant in average maximum voltage output. This specimen had a statistically lower average maximum voltage. It is important to note for all specimens the average maximum voltage occurred at the lowest resistance of 30 ohm for each one.

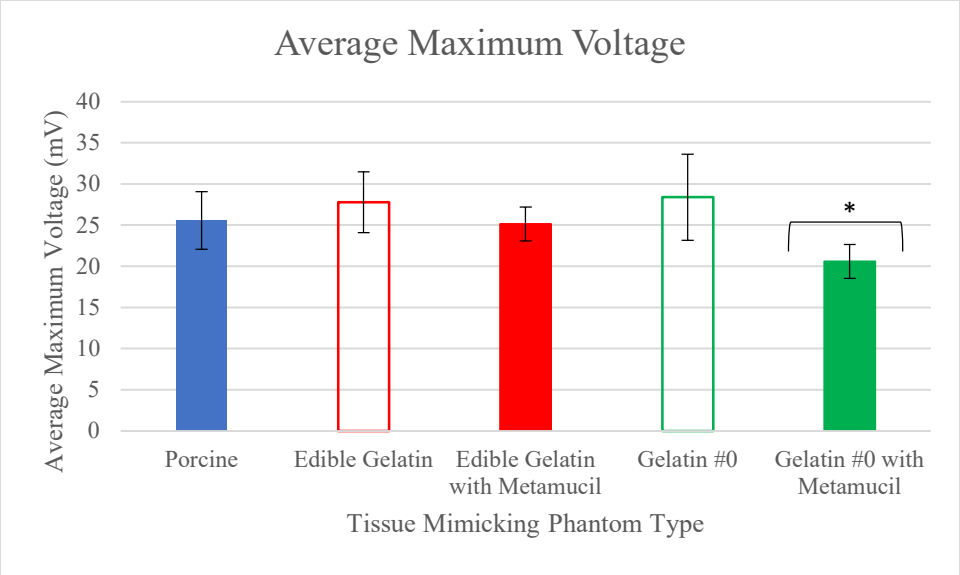

*Figure 18 - Average Maximum Voltage Output from the PZT for each phantom type. * Indicates statistically significant.*

The average voltage output at one kiloohm for all phantom types was compared to porcine. None of them were statistically different in voltage output at this resistance.

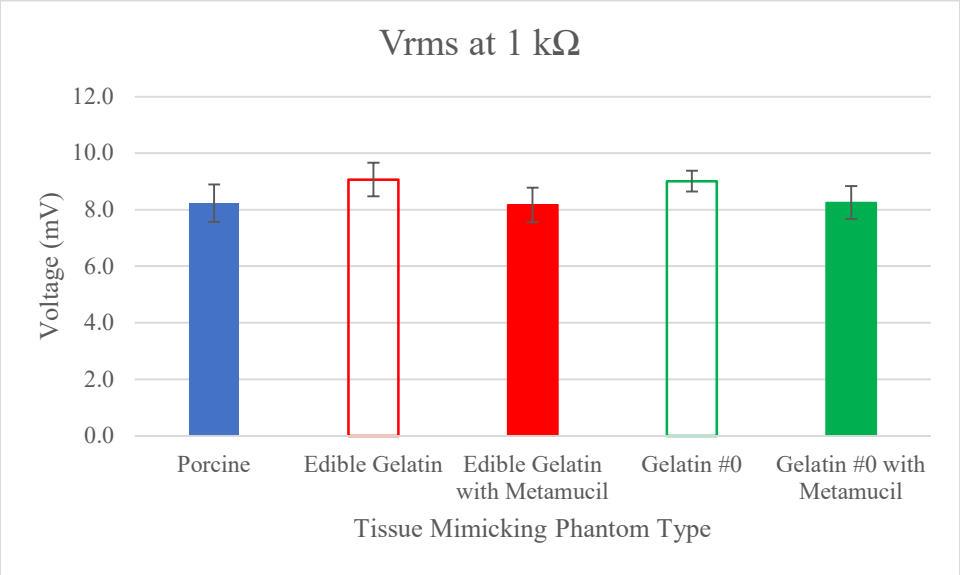

Figure 19 - Average Voltage Output from the PZT for each phantom type at one kiloohm.

A summary of the power and voltage outputs for each phantom type can be seen in Table 4. Although Gelatin #0 with Metamucil was statistically significant in power generation at 1000 ohms it had the smallest standard deviation.

*Table 7 - Power and Voltage Outputs for each Group. * indicates statistically significant.*

	Power Output (μW)		Voltage Output (mV)	
Group	Avg. Maximum ± Std. Dev.	Avg. at 1 kΩ ± Std. Dev.	Avg. Maximum ± Std. Dev.	Avg. at 1 kΩ ± Std. Dev.
Porcine	172 ± 55	73 ± 13	26 ± 3	8.2 ± 0.7
Edible Gelatin	205 ± 42	66 ± 14	28 ± 4	9.1 ± 0.6
Edible Gelatin with Metamucil®	146 ± 77	54 ± 19	25 ± 2	8.2 ± 0.6
Gelatin #0	270 ± 70	74 ± 27	28 ± 5	9.0 ± 0.4
Gelatin #0 with Metamucil®	109 ± 39	34 ± 11 *	21 ± 2 *	8.3 ± 0.6

It can be seen from the plot with all types of phantoms on it that the Gelatin #0 was the one with the greatest amount of power generation. This corresponds to the hypothesis that the lower attenuation would result in more of the intensity of the ultrasound striking the PZT disc. From preliminary studies more Metamucil® had to be added to the edible gelatin and it still was not statistically significant compared to the standard edible gelatin, suggesting more should be added.

3.5 Discussion

3.5.1 Comparing Tissue Phantoms

The goal of the application was to examine the differences between tissue phantoms. Parameters to consider when choosing a tissue phantom for this specific ultrasound and implanted piezoelectric study are acoustic properties, room temperature stability, number of uses, power output, and voltage. The acoustic properties of the phantom matter because the location of the implanted transcutaneous device. For this specific application the location is in the abdomen which is why the specific thicknesses were chosen from abdominal wall thicknesses of 40mm ± 2mm. This portion of anatomy will include skin, subcutaneous fat, and muscle making it a difficult tissue to mimic to the boundary changes and differences in attenuation. The attenuation for the gelatin #0 from the manufacture is 0.22 dB

3.5.2 Pros and Cons of the Phantoms

There are a variety of characteristics a tissue phantom must display and those will vary depending on application. For the specific application tested here of transcutaneous the ultrasound phantom must be similar in acoustic properties to skin, fat, and muscle, stable at room temperature, and reusable. The edible gelatin phantom was not statistically significant compared to porcine in power generation and voltage production at 1000 ohms (expected resistance of muscle). It was not statistically significant for average maximum power or voltage output. This type of homemade phantom has been used in the past as an ultrasound phantom to mimic skin and tissue but is unfortunately not able to be reused and cannot be left out at room temperature for long periods of time. The edible gelatin with the fiber additive was not statistically significant in power generation and voltage to the porcine model at 1000 ohms or for maximum power and voltage outputs. Similar studies have used this type of phantom for ultrasound studies, so it has similar acoustic properties to skin and subcutaneous tissue. However, it is not able to be left out at room temperature for long periods of time or able to be reused over multiple days.

Examining the average maximum power generation Gelatin #0 was not statistically different from the porcine. Gelatin #0 was not statistically significant to porcine power generation at 1000 ohms and voltage output at 1000 ohms. The acoustic characteristics, however, are manufactured for soft tissue with a lower attenuation than what would be seen with a full transcutaneous model including skin and muscle. It is expected this is why it was the highest power generation of all specimens because it had a lower attenuation allowing for more ultrasound intensity to load the disc. In addition, there were several runs on specimens were the voltage output would increase along with the power generation and this would result in a slight warmth at the disc. A thermocouple was used during one test to measure, but no increase by a degree was seen. However, since ultrasound coupling gel is water soluble it was speculated when this warmth happened and since there was contact between the encapsulated disc, coupling gel, and gelatin #0 at these locations small inclusions occurred. The disc and phantom would have to be rotated to avoid these inclusions for future testing runs. These inclusions were seen on runs where that jump in power and voltage occurred and were not seen at lower power generation runs.

For average maximum power generation gelatin #0 was not statistically significant compared to the porcine. However, gelatin #0 with the fiber addition was statistically significant to porcine for power generation at 1000 ohms but not for voltage output at 1000 ohms. The exact acoustic properties are unknown as ultrasound attenuation measurements were not performed but considering the difference in power generation compared to the other groups it is a higher attenuation. The power generation was significantly lower than that of the porcine. The voltage output for the purpose of providing current density to a hernia repair mesh was not statistically different so it could be used in that application even though the power generation is less. It is reusable and stable at room temperature. Perhaps a future study would include less fiber supplement and acoustic measurements performed on it.

3.5.3 Power Output Comparisons from Different Phantoms

The power generation is important as this displays how well the PZT is converting the electrical energy. For the average maximum power generation, no specimen was statistically significant compared to porcine.

However, for power generation at 1000 ohms where the overall resistance of muscle might be the grouping was different with all being statistically similar except gelatin #0 with Metamucil®. The difficulty is the two phantoms that are stable at room temperature are those that have gelatin #0, but the attenuation for the gelatin #0 is much lower than that of expected attenuation for the porcine model, but the power generation is still statistically similar for the average maximum power generation across the specimens in the groups.

3.5.4 Root Mean Square Voltage Comparison for Applications

The root mean square voltage production for the Gelatin #0 with Metamucil® was statistically different than the porcine for average maximum voltage produced. For applications that require a lower voltage for testing this would be an appropriate phantom to use to control that output. It is important to note the voltage produced by a single disc specimen with a 40 mm phantom has maximums in the ranges

of 21-28 mV depending on the type of phantom used and at a lower resistance with an ultrasound intensity of 1.0 W/cm^2. For implanted single disc devices with high frequency AC output, it is imperative to use an accurate resistance that the electrode will see in the body as there is a significant difference between the lower resistance voltage outputs and higher.

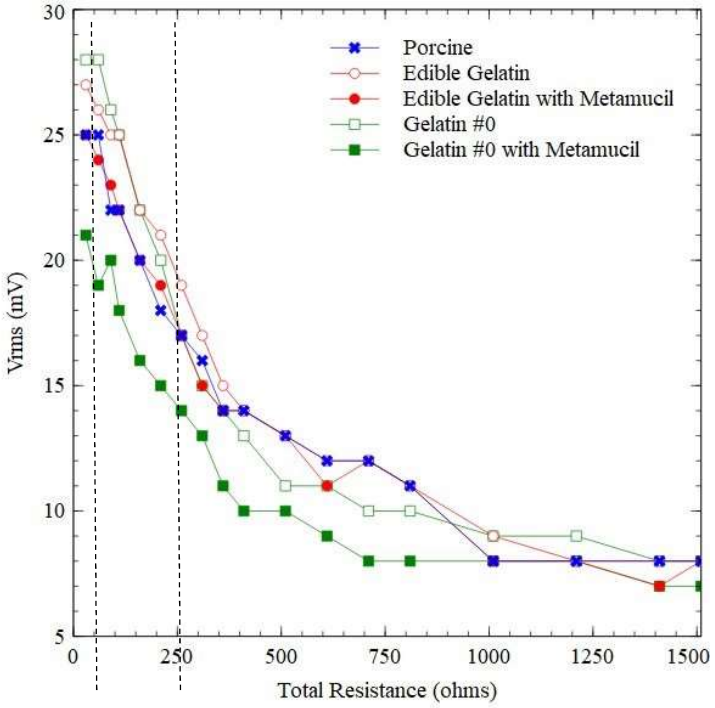

Figure 20 - Vrms vs. Total Resistance. The bars are marked at 50 and 250 ohms to show the range of voltages at lower resistances.

3.5.6 Hernia Repair Mesh Application

All phantoms were found to be statistically similar in root mean square voltage generation at 1000 ohms. However, the average maximum voltage for the Gelatin #0 with the fiber additive was statistically significant.

Although there is a difference in power output with the use of different phantoms the voltages at higher resistances those that the mesh could see being in the body are less different. The table for the current density for the given phantom can be seen below (Tables 6 and 7). Considering the resistance of

muscle and soft tissue is between 750-1000 ohms the values were taken at 800 ohms and 1000 ohms. These voltages since they will be in parallel with the mesh will be the same voltage drop across the mesh. That value can then be used to determine the current given the total resistance. A total calculated electrode area of 39.87 cm^2 was used and for this example was divided into six individually smaller areas to be used with a well plate. The theoretically calculated values can be seen below.

Table 4 - Ultrasound Intensity 1.0 W/cm^2. 800-ohm resistor used in addition to 10-ohm.

800-ohm Maximum current Density 6 Well Plate			
Phantom	**RMS Voltage (mV)**	**Current Density (nA/cm^2)**	**Std. Dev.**
Porcine	11.0	57.5	1.61
Edible Gelatin	11.0	57.5	1.8E-15
Edible Gelatin + Metamucil	10.9	57.0	0.56
Gelatin Zero	9.6	50.2	1.09
Gelatin Zero + Metamucil	8.1	42.3	1.06

Table 5 - Ultrasound Intensity 1.0 W/cm^2. 1000-ohm resistor used in addition to 10-ohm.

1000-ohm Minimum current Density 6 Well Plate			
Phantom	**RMS Voltage (mV)**	**Current Density (nA/cm^2)**	**Std. Dev.**
Porcine	8.3	34.7	0.66
Edible Gelatin	9.0	37.6	0.55
Edible Gelatin + Metamucil	8.2	34.3	0.61
Gelatin Zero	9.1	38.0	0.38
Gelatin Zero + Metamucil	8.3	34.7	0.67

A limitation to these calculations is the area is an estimation and there is more variability in voltages at lower resistances across the phantoms. For the future cellular studies, the solutions resistance would need to be measured to determine the actual current density delivered. Circuit diagrams and the application connected to well plates can be seen in the figure below.

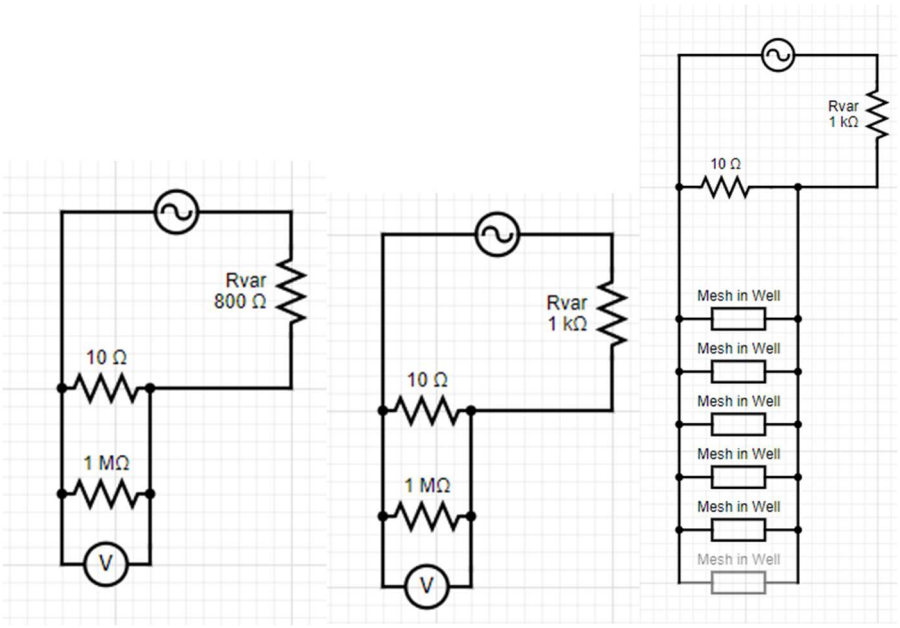

Figure 21 - Circuit diagrams of studies resistance sweep and future benchtop testing with hernia repair mesh in solution.

3.6 Conclusion

This study investigates different types of tissue mimicking materials for transcutaneous stimulation by ultrasound of a single PZT disc. Being able to identify which tissue phantoms are like that of porcine tissue that includes skin, fat, and muscle is important in replicating ultrasound characteristics *in vitro*. All materials chosen and ultrasound settings have been seen in literature to be clinically relevant for tissue mimicking materials and medically safe therapeutic ultrasound. The ability to be able to use a clinically relevant phantom for further transcutaneous ultrasound testing to load a piezoelectric material could be important for future directions of this technology.

Research in the future could use these phantoms with different piezoelectric composite materials to achieve desired maximum power output and voltage output for desired implant location. This study strictly focused on phantoms that were of thickness and relevance to the abdomen area, but future studies could change desired thickness and ultrasound parameters to achieve desired outcomes of power and voltage.

3.7 Acknowledgements

The authors would like to thank, Ember Krech, Morghan Alters, Tori Drapal, Morgan Riley, Luke Lindemann, Ryan Downing, and Savannah Mosier at the University of Kansas for their advice and assistance on this project.

3.8 Funding Data

This work was supported by the SHARPHub Grant: 1002191

3.9 Nomenclature

PZT – Lead Zirconate Titanate

AC – Alternating Current

DC – Direct Current

ANOVA – Analysis of Variance

RMS – Root Mean Square

Chapter 4: Conclusions and Future Work

4.1 Conclusions

All tissue phantoms were not statistically different in average maximum power generation. Gelatin #0 with fiber additive was statistically significant in power generation at 1000 ohms. For voltage output at 1000 ohms none of the phantoms were statistically different compared to the porcine. Gelatin #0 with fiber additive was statistically different in maximum voltage output compared to porcine. The edible gelatin phantoms with additives were closer to a porcine tissue model in power generation as they provided more clinically relevant attenuation to the controlled ultrasound intensity. A single PZT disc can generate the prescribed current density to a hernia repair mesh. Future studies will judge whether that current density at the unchanged output frequency enhances healing.

4.2 **Limitations**

Ultrasound beam from this specific therapeutic ultrasound device is naturally a nonhomogeneous acoustic beam. This can be described by a specific ratio by the name of beam non-uniformity ratio. For this specific probe that ratio is 5:1 corresponding to the highest intensity on the face of the probe and the lowest. In addition, although the locations of the phantom orientation, disc, and probe were marked there was a small degree of variation between runs because the disc was removed from the location. It was removed after each run to check capacitance and rested for 15 minutes between resistance sweeps. These two factors together could result in variation of the amount of energy transferred from the ultrasound to the PZT. Lastly, although the phantoms were all mixed according to the recipes and there is small variation between the specimens with the fiber additives due length in oven for air bubble removal and length in fridge for setting time.

4.3 Future Work

Further ultrasound acoustic measurements of properties of the phantoms with additives could be performed. Reducing the amount of Metamucil® in the Gelatin #0 could be performed until it reaches a power generation at all resistances that is not statistically significant. The project has many options to move forward with the technology. In addition, with the knowledge from this study could be used for a cellular and an in-depth study exploring the effect of frequency and precision-controlled circuit on an optimal signal for specific muscle sells for healing. The avenue of different electrode materials could be explored and additional applications for diabetic ulcers or other prosthetic meshes take the base technology.

4.4 References

1. Kulacoglu, H., *Current options in inguinal hernia repair in adult patients.* Hippokratia, 2011. **15**(3): p. 223-231.
2. Poulose, B., et al., *Epidemiology and cost of ventral hernia repair: making the case for hernia research.* The World Journal of Hernia and Abdominal Wall Surgery, 2012. **16**(2): p. 179-183.
3. Burger, J.W.A., et al., *Long-term follow-up of a randomized controlled trial of suture versus Mesh repair of incisional hernia. Discussion*. 2004, Hagerstown, MD: Lippincott: Hagerstown, MD. p. 578-585.
4. Langbach, O., et al., *Long-term quality of life and functionality after ventral hernia mesh repair.* Surg Endosc, 2016. **30**(11): p. 5023-5033.
5. Lange, B., et al., *Mesh penetration of the sigmoid colon following a transabdominal preperitoneal hernia repair.* Surg Endosc, 2003. **17**(1): p. 157-1.
6. Alters, M., *Determination of Clinical Efficacy of Ultrasound Stimulation on Piezoelectric Composites for Power Generation Applications*, E. Friis, C. Luchies, and L. D'Silva, Editors. 2019, University of Kansas.
7. Carmine Wang, S., K. Tiffany, and Z. Donghui, *Hernia Mesh and Hernia Repair: A Review.* Engineered Regeneration, 2020. **1**: p. 19-33.
8. O'Dwyer, P., et al., *Laparoscopic versus open repair of groin hernia: a randomised comparison.* Lancet, 1999. **354**(9174): p. 185-190.
9. Baylón, K., et al., *Past, Present and Future of Surgical Meshes: A Review.* Membranes, 2017. **7**(3).
10. Rognoni, C., et al., *Budget Impact Analysis of a Biosynthetic Mesh for Incisional Hernia Repair.* Clinical Therapeutics, 2018. **40**(11): p. 1830-1844.e4.
11. Ud-Din, S., et al., *Angiogenesis is induced and wound size is reduced by electrical stimulation in an acute wound healing model in human skin.* PloS one, 2015. **10**(4): p. e0124502-e0124502.
12. Bhang, S.H., et al., *Zinc Oxide Nanorod-Based Piezoelectric Dermal Patch for Wound Healing.* Advanced Functional Materials, 2017. **27**(1): p. n/a-n/a.
13. Sanders, D. and A. Kingsnorth, *From ancient to contemporary times: a concise history of incisional hernia repair.* The World Journal of Hernia and Abdominal Wall Surgery, 2012. **16**(1): p. 1-7.
14. Dowell, G., *A treatise on hernia: with a new process for its radical cure, and original contributions to operative surgery, and new surgical instruments. By Greensville Dowell*. 1876, Pennsylvania: Pennsylvania: D.G. Brinton, 1876.
15. Nyhus, L.M., et al., *The preperitoneal approach and prosthetic buttress repair for recurrent hernia. The evolution of a technique.* Annals of surgery, 1988. **208**(6): p. 733.
16. Usher, F.C. and S.A. Wallace, *Tissue Reaction to Plastics: A Comparison of Nylon, Orlon, Dacron, Teflon, and Marlex.* A.M.A. archives of surgery, 1958. **76**(6): p. 997-999.
17. Arnaud, J.-P. and P. Pessaux, *Surgical treatment of postoperative incisional hernias by intraperitioneal insertion of Dacron mesh and an aponeurotic graft.* Archives of Surgery, 1999. **134**(11): p. 1260-2.
18. Kingsnorth, A., *The management of incisional hernia.* Annals of The Royal College of Surgeons of England, 2006. **88**(3): p. 252-260.
19. Deerenberg, E., et al., *A systematic review of the surgical treatment of large incisional hernia.* The World Journal of Hernia and Abdominal Wall Surgery, 2015. **19**(1): p. 89-101.
20. La Mura, F., et al., *Emergency treatment of complicated incisional hernias: a case study.* Annals of surgical innovation and research, 2009. **3**(1): p. 15-15.
21. Den Hartog, D., et al., *Open surgical procedures for incisional hernias.* Cochrane Database Syst Rev., 2008(3).

22. Leblanc, K., *The critical technical aspects of laparoscopic repair of ventral and incisional hernias.* The American Surgeon, 2001. **67**(8): p. 809-12.
23. Pans, A., et al., *Long-term results of polyglactin mesh for the prevention of incisional hernias in obese patients.* World J.Surg., 1998. **22**(5): p. 479-483.
24. Trimbos, J.B., et al., *A Randomized Clinical Trial Comparing Two Methods of Fascia Closure Following Midline Laparotomy.* Archives of surgery (Chicago. 1960), 1992. **127**(10): p. 1232-1234.
25. Luijendijk, R.W., et al., *A comparison of suture repair with mesh repair for incisional hernia.* The New England journal of medicine, 2000. **343**(6): p. 392-398.
26. Raptis, D.A., et al., *A Comparison of Woven Versus Nonwoven Polypropylene (PP) and Expanded Versus Condensed Polytetrafluoroethylene (PTFE) on Their Intraperitoneal Incorporation and Adhesion Formation.* The Journal of surgical research, 2011. **169**(1): p. 1-6.
27. Greca, F., et al., *The influence of porosity on the integration histology of two polypropylene meshes for the treatment of abdominal wall defects in dogs.* The World Journal of Hernia and Abdominal Wall Surgery, 2008. **12**(1): p. 45-49.
28. Orenstein, S.B., et al., *Comparative Analysis of Histopathologic Effects of Synthetic Meshes Based on Material, Weight, and Pore Size in Mice.* The Journal of surgical research, 2012. **176**(2): p. 423-429.
29. Lee, L.H., *Randomized clinical trial of groin hernia repair with titanium-coated lightweight mesh compared with standard polypropylene mesh (Br J Surg 2008*

95: 1226–1231. British Journal of Surgery, 2009. **96**(2): p. 221-221.
30. Rouabhia, M., et al., *Electrical stimulation promotes wound healing by enhancing dermal fibroblast activity and promoting myofibroblast transdifferentiation.* PloS one, 2013. **8**(8): p. e71660.
31. Ward, A., *Electrical Stimulation Using Kilohertz-Frequency Alternating Current.* Phys. Ther., 2009. **89**(2): p. 181-190.
32. Kim, T.H., H.-y. Cho, and S.M. Lee, *High-Voltage Pulsed Current Stimulation Enhances Wound Healing in Diabetic Rats by Restoring the Expression of Collagen, α-Smooth Muscle Actin, and TGF-β1.* The Tohoku Journal of Experimental Medicine, 2014. **234**(1): p. 1-6.
33. Koh, K., *Effects of alternating current electrical stimulation on the cellular chemistry and proliferation of C2C12 muscle cells*, D. Nawarathna, D. Ewert, and T. Gustad, Editors. 2016, ProQuest Dissertations Publishing.
34. APC International, L., *Piezoelectric Ceramics: Principles and Applications.* APC International., 2011.
35. Ahmadi, F., et al., *Bio-effects and safety of low-intensity, low-frequency ultrasonic exposure.* Progress in biophysics and molecular biology, 2012. **108**(3): p. 119-138.
36. McGarry, C.K., et al., *Tissue mimicking materials for imaging and therapy phantoms: a review.* Physics in medicine and biology, 2020.
37. Krech, E., *Leading the Charge in Bone Healing: Design of Compliant Layer Adaptive Composite Stacks for Electrical Stimulation in Orthopedic Implants*, E. Friis, et al., Editors. 2020, ProQuest Dissertations Publishing.
38. Li, H., C. Tian, and Z.D. Deng, *Energy harvesting from low frequency applications using piezoelectric materials.* Applied Physics Reviews, 2014. **1**(4).
39. Goetzinger, N.C., et al., *Composite piezoelectric spinal fusion implant: Effects of stacked generators.* Journal of Biomedical Materials Research Part B: Applied Biomaterials, 2016. **104**(1): p. 158-164.
40. Yang, Y., et al., *Optimization of low-frequency low-intensity ultrasound-mediated microvessel disruption on prostate cancer xenografts in nude mice using an orthogonal experimental design.* Oncology letters, 2015. **10**(5): p. 2999.

41. Koch, T., et al., *Ultrasound velocity and attenuation of porcine soft tissues with respect to structure and composition: I. Muscle.* Meat science, 2011. **88**(1): p. 51-58.
42. Koch, T., et al., *Ultrasound velocity and attenuation of porcine soft tissues with respect to structure and composition: II. Skin and backfat.* Meat science, 2011. **88**(1): p. 67-74.
43. Techavipoo, U., et al., *Temperature dependence of ultrasonic propagation speed and attenuation in excised canine liver tissue measured using transmitted and reflected pulses.* J Acoust Soc Am, 2004. **115**(6): p. 2859-2865.
44. Dong, D.-H., et al., *Study of Individual Characteristic Abdominal Wall Thickness Based on Magnetic Anchored Surgical Instruments.* Chinese Medical Journal, 2015. **128**(15): p. 2040-2044.
45. Miller, D.L., et al., *Overview of Therapeutic Ultrasound Applications and Safety Considerations*. 2012. p. 623-634.
46. Techavipoo, U., et al., *Temperature Dependence of Ultrasonic Propagation Speed and Attenuation in Canine Tissue.* Ultrasonic imaging, 2002. **24**(4): p. 246-260.
47. Miao, L., et al., *Physical Characteristics of Medical Textile Prostheses Designed for Hernia Repair: A Comprehensive Analysis of Select Commercial Devices.* Materials (Basel, Switzerland), 2015. **8**(12): p. 8148-8168.
48. Schwan, P.H. and F.C. Kay, *Specific Resistance of Body Tissues.* Circulation Research, 1956. **4**(6): p. 664-670.

Appendix A: Supplementary Figures

Additional Plots

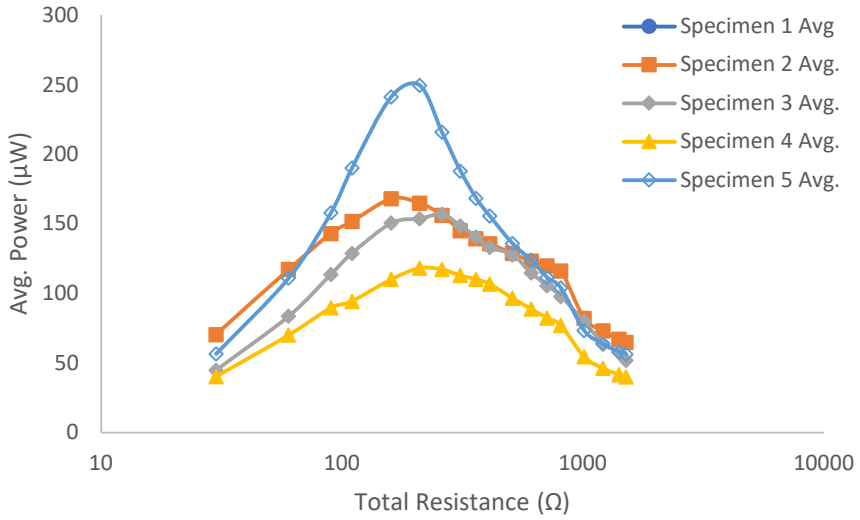

Figure 3 - Average Power vs. Total Resistance. Porcine Specimen Averages. Average of all 6 runs for each specimen were taken. Ultrasound Intensity of 1.0 W/cm^2.

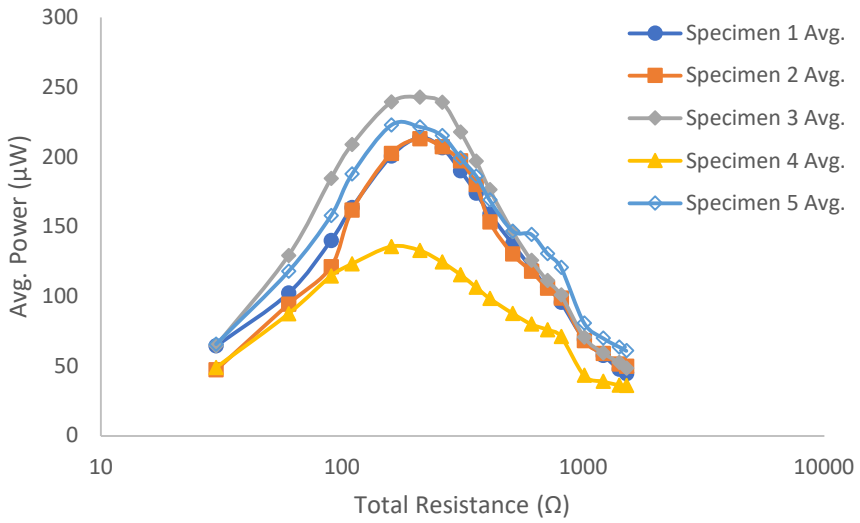

Figure 4 - Average Power vs. Total Resistance. Edible Gelatin Specimen Averages. Average of all 6 runs for each specimen were taken. Ultrasound Intensity of 1.0 W/cm^2.

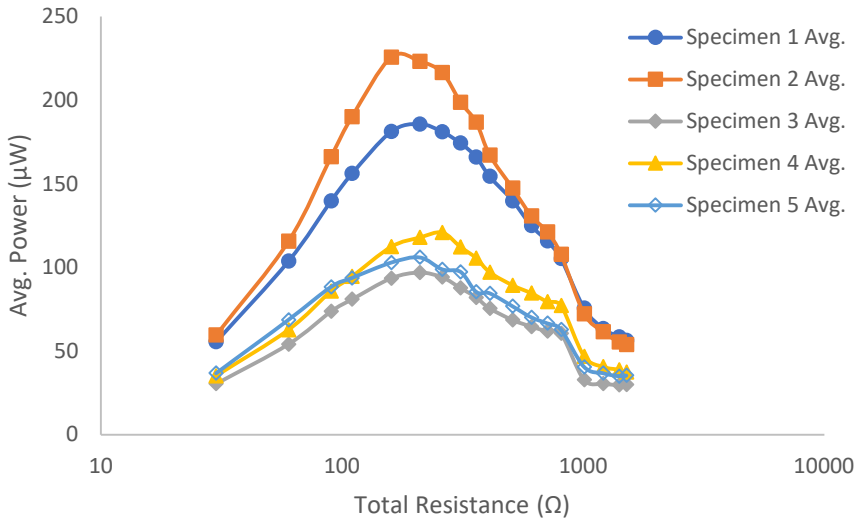

Figure 5 - Average Power vs. Total Resistance. Edible Gelatin + Metamucil Specimen Averages. Average of all 6 runs for each specimen were taken. Ultrasound Intensity of 1.0 W/cm^2.

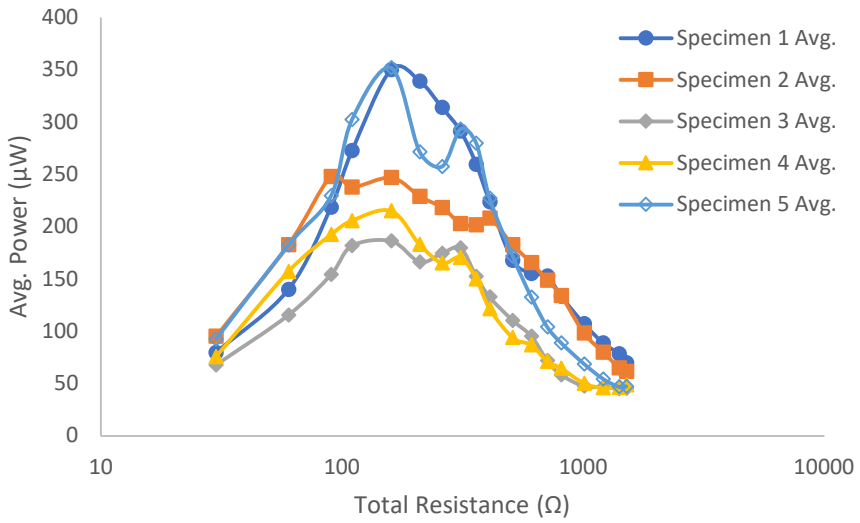

Figure 6 - Average Power vs. Total Resistance. Gelatin Zero Specimen Averages. Average of all 6 runs for each specimen were taken. Ultrasound Intensity of 1.0 W/cm².

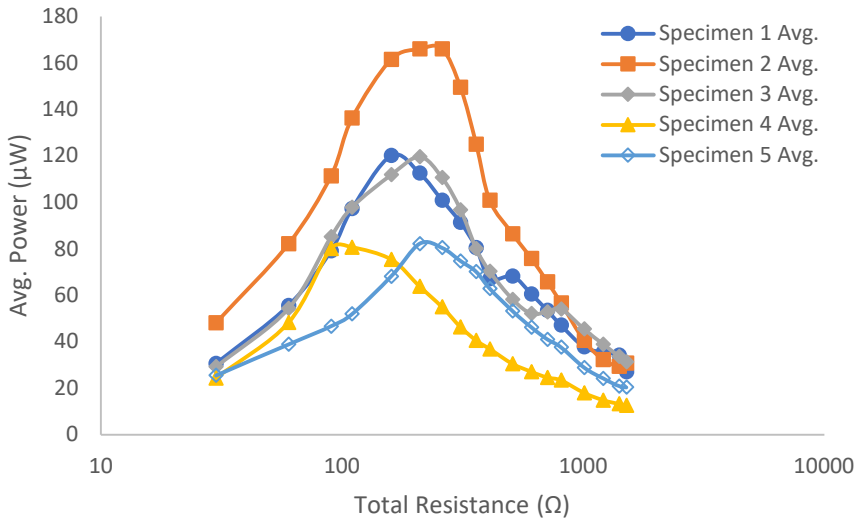

Figure 7 - Average Power vs. Total Resistance. Gelatin Zero + Metamucil Specimen Averages. Average of all 6 runs for each specimen were taken. Ultrasound Intensity of 1.0 W/cm².

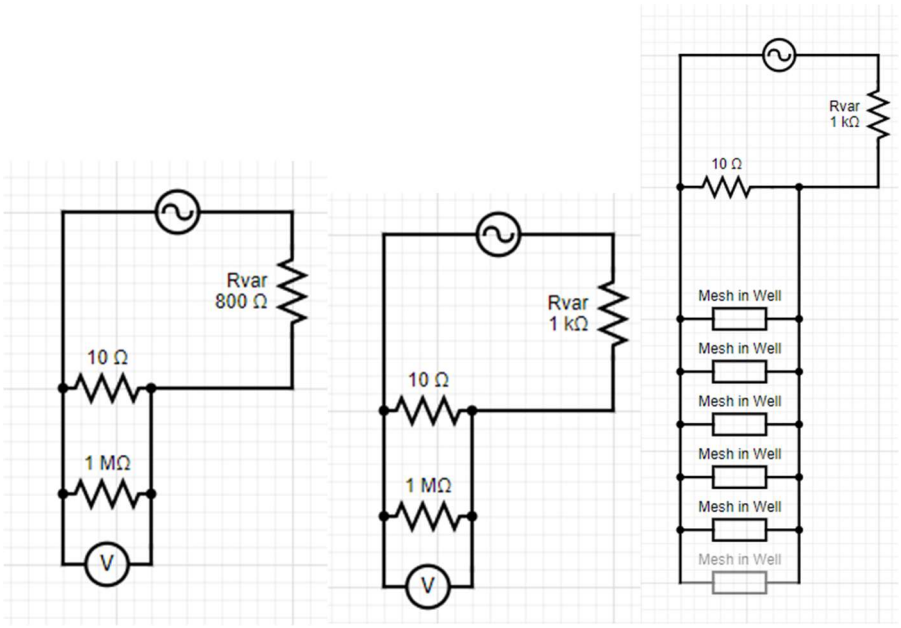

Figure 8 - Circuit Diagrams for testing and for application with meshes in well plate with all parallel meshes.

Additional Tables

Specimen	Skin (mm)	Fat (mm)	Muscle (mm)	Total Height (mm)
1	3	20	15	38
2	4	14	24	42
3	4	20	16	40
4	4	20	18	42

Specimen	Muscle R Values (MΩ)	Fat R Values (MΩ)	Avg. R Muscle (MΩ)	Avg. R Fat (MΩ)
2	0.356	0.689	0.5274	0.8858
	0.436	0.937		
	0.747	1.007		
	0.33	0.834		
	0.768	0.962		
5	0.883	1.001	0.8288	1.0034
	0.741	0.892		
	0.806	1.014		
	0.981	1.068		

	0.733	1.042		
		Total Averages	0.6781	0.9446

800-ohm Maximum current Density 6 Well Plate			
Phantom	**RMS Voltage (mV)**	**Current Density (nA/cm^2)**	**Std. Dev.**
Porcine	11.0	57.5	1.61
Edible Gelatin	11.0	57.5	1.8E-15
Edible Gelatin + Metamucil	10.9	57.0	0.56
Gelatin Zero	9.6	50.2	1.09
Gelatin Zero + Metamucil	8.1	42.3	1.06

1000-ohm Minimum current Density 6 Well Plate			
Phantom	**RMS Voltage (mV)**	**Current Density (nA/cm^2)**	**Std. Dev.**
Porcine	8.3	34.7	0.66
Edible Gelatin	9.0	37.6	0.55
Edible Gelatin + Metamucil	8.2	34.3	0.61
Gelatin Zero	9.1	38.0	0.38
Gelatin Zero + Metamucil	8.3	34.7	0.67

Hernia Repair Mesh given a 175 cm^2 surface area with a 55.7% porosity to give an electrode surface area of 77.5 cm^2 current density tables.

800-ohm Maximum current Density Hernia Repair Mesh			
Phantom	**RMS Voltage (mV)**	**Current Density (nA/cm^2)**	**Std. Dev.**
Porcine	11.0	177.4	1.61
Edible Gelatin	11.0	154.8	1.8E-15
Edible Gelatin + Metamucil	10.9	130.6	0.56
Gelatin Zero	9.6	175.7	1.09
Gelatin Zero + Metamucil	8.1	177.4	1.06

1000-ohm Minimum current Density Hernia Repair Mesh			
Phantom	**RMS Voltage (mV)**	**Current Density (nA/cm^2)**	**Std. Dev.**
Porcine	8.3	107.1	0.66
Edible Gelatin	9.0	117.4	0.55
Edible Gelatin + Metamucil	8.2	107.1	0.61

Gelatin Zero	9.1	105.8	0.38
Gelatin Zero + Metamucil	8.3	116.1	0.67

Appendix B Detailed Methods

Single Disc Construction for hernia repair and phantom testing

1. Choose desired PZT disc.
2. Verify poling direction. The discs I used were a fellow lab mates' old discs. He had marked the positive side, but to make sure. You can test it. Many manufactures will also mark the positive side of the discs, but it is good practice to always verify before fabricating.
3. The discs I used were marked by a small pencil circle for the positive side.
4. To test, place an aluminum sheet on an insulator on the table. Then place the disc negative side down on the aluminum sheet metal.
5. Set a multimeter to DC voltage and without scratching the PZT place the positive lead (red) to the face of the positive side of the disc and place the negative lead (black) to the aluminum sheet metal.
6. With these connections exhale a quick puff of air on the disc and if the multimeter reads a + DC voltage then the disc is marked correctly. If the opposite occurs then it is incorrectly marked, so correct the marking by using a different color on the actual positive side and not in your procedure.
7. Repeat this for all the discs you plan to fabricate.

Electrical connection for Single discs

1. You need to connect wires to the disc. For this study I used the thin electrical wires that were colored.
2. Begin heating the oven it needs to be 130 °C.
3. Lay a disc on a rectangular piece of Delrin with positive side facing upward. This is just for one disc but you can do more than one at a time.
    a. For two discs set both discs with positive side facing upward and you will lay wire across both discs. And then flip and follow the same procedure for the negative side. This connects the discs electrically in parallel. This is different than the stacks because the electrically parallel discs are in the same plane. You could add more discs if needed. For this project we ended up going with a single disc, but tested out several double disc setups.
4. Take some conductive epoxy (EPO-TEK ®H20E) out of the freezer, use gloves while handling this as it toxic. Using the end of a Q-tip that has been narrowed place a dab on the disc and place them on top. Place another small dab on-top of the wire to ensure a connection. Be careful to not use too much as conductive epoxy is incredibly expensive and you do not want any overflow. Tweezers can help with placement.
5. Once wire is in position place a round red silicone piece on top using tweezers. Be sure not to jostle the wire as this can mess up the connection. Place a small metal nut to act as a weight on top of this again be delicate.
6. Then when oven is to temperature place in the oven for 30 minutes at 130 °C.
7. Once curing in the oven is completed take out and let cool for about 15-20 minutes for these small discs. If discs are larger and thicker this could take more time.
8. Following cooling carefully remove the weight and very gently take silicone piece off, this can very easily remove the wire connection if it has not cooled enough so be careful.
9. Verify the connection is complete by using a multimeter.
10. Flip disc to negative side and repeat the above steps. Be sure to offset the wires to decrease chances of touching.

11. Following both sides connected use the LCR to determine if the connection is complete and right down the values of capacitance, impedance, and resistance for further fabrication step verifications.
12. Connection verification can also be done by placing on a silicone mat and connecting wires to a voltmeter set to read resistance. If you get over load, O.L. all connections have been done correctly.
13. Check wire connection to disc by using the voltmeter set to resistance again place one lead of the multimeter on the wire and the other on the face of the PZT disc of the same pole, the multimeter should output a low resistance value.
14. Repeat for all single discs you have connected electrically.

Attachment to Petri Dish

1. For this study the disc was attached to a petri dish as a hard backing to keep the disc in place for testing of all phantoms. This was especially convenient when working with the pig tissue.
2. Following the wiring and verifying electrical connection stir the rubber cement. The instructions are on the bottle.
3. Place a dab on the side of the disc you want face down and a dab on the petri dish. The instructions state to let these sit until glossy 15 minutes to 2 hours no longer than 2 hours. For the amount I used it took about 20-30 minutes, but watch carefully.
4. Once glossy you can stick the two surfaces together. Be careful to keep the disc level
5. The setting process takes several hours

Silicone Encapsulation of the Disc

1. Mix up dragon skin silicone according to manufacture instructions
2. The ratio of Part A to Part B is 1:1
3. Once mixed use as quickly as you can being careful to check for air bubbles
4. Wait a few minutes and as it begins to set carefully move any air bubbles that are over the disc to the side. You do not want any bubbles over the disc as this impedes the ultrasound greatly.
5. Allow 2 hrs. to fully cure
6. When cleaning between runs from the coupling gel use be careful to dab clean and not try to scrub as the silicone can be peeled off from the petri dish and would then need to be replaced.

Ultrasound and Oscilloscope Testing Technique

1. Turn on the oscilloscope and insert your flash drive in the USB port
2. Turn on the ultrasound machine to load and warm up.
3. Set the oscilloscope data collection to 100MS/s and number of points collected to 10k and 10µs.
4. The setup is saved under May XXXX which allows you to see instantaneous values as well.
5. The save button for this setup is set to save waveform, click menu and then “save assign waveform” to see what the file name is. I note this file name and then change on my computer later if needed. Do this before each run of a resistance sweep so you know which data files are yours. The setting should also be setup for .csv. The manual is helpful if this ever gets erased.
6. Click channel 1 button and then probe and then keep clicking that same button until you see probe setup. If using the cable, the attenuation needs to be 1x if using the differential probe, you need to allow the oscilloscope to adjust for this, so it needs to be 10x.
7. Connect the cable with the 10ohm resistor across it. By connecting this resistor in parallel with the oscilloscope channel 1 that has a resistance of 1M ohm then makes the impact of the 1 M ohm resistance of the oscilloscope negligible

8. For this study I used a height of 40 mm to reach the ultrasound transducer face.
9. The ultrasound probe is held in place by a vice with the transducer face parallel to the plane of the disc and phantom. It is important the plane of the disc, phantom, and transducer are all parallel to optimize the mechanical waves from the transducer striking the face of the disc.
10. Place a small bit of coupling gel on top of the disc in order to mitigate the barrier between the disc and your phantom. Place some coupling gel on the face of the U.S. transducer. Once the phantom and ultrasound transducer are all lined up. Mark where the phantom lies on top of the disc about the petri dish, so when the phantom is removed from the petri dish post a trial run it can be placed in the exact same position for the next trial.
11. Mark where your blocks are so they stay in position as well.
12. Connect the positive wire from the cable with the 10ohm resistor to the positive of the resistance box. Then connect the negative of the resistance box to the positive of the disc, and the negative of the disc to the negative of the cable. Although the positive and the negative sides of the discs do not matter this keeps the setup of each run the same.
13. **insert circuit diagram including the oscilloscope resistance
14. Once everything is connected you will see some slight noise on the oscilloscope that is normal.
15. Make sure the ultrasound machine is set continuous duty cycle, frequency of 1MHz, and then increase your intensity using the arrow buttons to the desired value. For this study it was 0.5 W/cm^2.
16. Turn your resistance box to your first value of resistance. Turn on the ultrasound probe on and move the phantom and disc setup in order to find the "sweet spot" by watching the voltage output till you see the spot that it is the highest. If you suspect the highest you see is lower than what you expect after the 15 seconds. Re adjust to the ultrasound transducer so the transducer face is as parallel as you can get it to the disc. If it slightly tilted upward or is too tight on the plane of the phantom that can impact the disc output.
17. Once the probe is set use the blue tape to arc over the probe to the table or edge of the block in order to hold it in place, so it doesn't tilt upward as the test goes on. It does not need to be too tight just a firm hold. At this point you have done either 1 or 2 intervals of stimulation on the disc. For this study I found that 5 of these stimulations of 15 seconds on and then 15 seconds off allowed for the disc and ultrasound to "warm up" and by the 4^{th} or 5^{th} one the waveform is holding steady at a value. Do not save these points they are just warm up. The 6^{th} stimulation will be the start of your resistance sweep. Following the 15 seconds waveform, pause the ultrasound probe wait 15 seconds no stimulation, start ultrasound again. Be sure to pause the ultrasound transducer and not hit the "stop" button as the stop button sets the intensity back to zero and then you have to warm it up again.
18. Repeat the start and pause for the remaining resistances in the sweep.
19. Once finished stop the ultrasound machine and disconnect the disc wires.
20. Remove the phantom and wipe off any coupling gel on the phantom and disc.
21. Set a timer for 15 minutes to let the PZT disc rest.
22. Once wiped off test the disc on the LCR the values these should be close to pre-testing. If they are not and the impedance matches the resistances you have a connection issue and/or possible short. This can happen with the thin wires connected on the disc, so be careful when handling and connecting and disconnecting them.
23. Following the 15 minutes of rest, test the disc on the LCR again for the pre-test for the next run and then repeat steps 10-22 for the remaining trial runs.

Tissue Phantoms

Determining the types of tissue phantoms was key in trying to best mimic tissue. For a control 5 porcine specimens were chosen. These tissue samples came from loin of the pig and consisted of skin on and all layers were maintained. They were carefully cut to size to fit within the petri dish over the encapsulated disc. All tissue samples were 40 mm tall when relaxed and the layers of skin, subcutaneous fat, and muscle were measured and recorded respectively. Total heights were the same but given the limitations of the porcine specimens there was some variability in thickness of fat and muscle. For testing purposes, a Styrofoam cup with large diameter of eight cm and small diameter of six cm was placed around the tissues on the petri dish to providing a boundary. One sample was tested at the beginning without a boundary and it was determined this provided too much movement when the probe was placed flushed. When over the disc freely it was speculated there was some shearing at the boundaries of tissues making for inconsistent results and some form of grounding or fastening was needed to hold the specimen in place for testing.

Gelatin #0 Humimic® Manufacturing Medical Ultrasound Phantoms

The gelatin #0 came from the manufacture Humimic® and was chosen as it is manufactured to match the acoustic properties of soft fatty tissue. The values for soft tissue, soft tissue fat, and muscle can be seen in table one. The values for Humimic® can be seen in table two. It is noted that the attenuation for the gelatin #0 is closest to the soft tissue fatty values with a low attenuation. It was hypothesized this will result in a higher power output seen for the gelatin 0 specimens as this phantom has the lowest attenuation. The attenuation of ultrasound is frequency independent and is only affected by the depth and the material type of the medium. These gelatin specimens were created by melting the gelatin at 130 °C (266 °F) for 4 hours in the oven per manufacture instructions. A benefit of this gelatin phantom is it is stable at room temperature and can be melted down up to 5 times while maintaining its acoustic characteristics. A silicone cupcake mold of 42 mm tall was used to create the specimen, this allowed for

easy clean-up and release of the mold. The gelatin was filled just below the rim at ~40 mm. By allowing the mold to be heated in the oven all the air bubbles were able to come to the top and be expelled. The mold is then taken from the oven and allowed to cool for 24 hrs.

Gelatin #0 Mold Creation Protocol

1. Set oven to 270 F, 132.2 C.
2. Clean inside of pink 6 x 6 cm silicone baking mold and let air dry completely
3. Same procedure whether using already melted or new gelatin #0
4. Cut squares of gelatin #0 and place in mold try not to pile too high above the mold, but make sure it is packed in there.
5. Do not go above ~110 g with container and gelatin.
6. Use clean gloves when handling gelatin to prevent from leaving residue in it.
7. Place in oven for 3-4hrs check after 10 min to ensure it is not overflowing on the edges if piled too high
8. If air bubbles are gone after 3 hrs. let cool 24 hrs. covered with something heat proof to keep dust particles off.
9. If remelted used gelatin note the date and the number of times it has been melted on the bag it was found in.
10. If new gelatin melted start a new bag and note the date of first melt down time.

Gelatin #0 Mold + Metamucil Protocol

1. Measure 8.6 g of sugar free Metamucil
2. Follow above steps for gelatin #0 1-7 at 3hrs take out and mix in Metamucil
3. Stir to combine working carefully yet still quickly as the gelatin will begin to set when out of the heat source. Once well mixed place back in oven for another 1 hr.
4. Remove from oven after 1 hr. use a paper towel to carefully remove the top layer of bubbles careful to not remove too much gelatin #0.
5. Place back in oven for another 45 minutes take out and stir as the Metamucil begins to settle at the bottom.
6. Place back in oven for another 45 minutes check and move any bubbles to the side and remove from the oven to set. There should be a gradient of Metamucil. If too much settled at the bottom good results will not be seen.

Edible Gelatin

The store-bought unflavored gelatin was the same recipe as seen in Alters et. al. with a ratio of approximately 10:1 water to gelatin, mL of water to g of gelatin. Gelatin has been an easy tissue mimicking phantom as it is readily available and can be controlled based on the ratios of gelatin and water mixed up. This phantom is expected to provide more attenuation than that of the gelatin 0. This mold is created by using distilled or de-ionized water, 277 mL and 27.2 g of gelatin and heated for 10 minutes over a hot plate and mixed. It is cooled for 30 minutes before being poured in a silicone cupcake mold that had has the opaque bottom removed and replaced with plastic wrap. Alters et. al. cites the gelatin and plastic wrap combination to mimic skin and tissue [6]. The mixture is then cooled in the fridge for up to 2 hrs. and tested with. No samples were allowed more than 24 hrs. before testing as the gelatin can begin to degrade and is not stable to be left at room temperature. In between all testing the gelatin was placed in the fridge for the 15 minutes in between runs. Edible gelatin mold had to remain in the silicone cupcake in order to maintain its integrity, so the orientation of this mold for both this and edible gelatin + Metamucil® was the slightly smaller diameter on the bottom over the disc (upright position) and did not have the Styrofoam cup as it was in the silicone mold. It is not expected this geometry affected the ultrasound as the height was the same and the ultrasound probe face was still smaller than the base diameter. The volume was the same as that used in gelatin 0 and all Metamucil® samples.

Store-bought Unflavored Gelatin Phantom

1. Using unflavored gelatin for phantom creation. The Single packets are easiest to use but a container of powder can also be used, as long it is unflavored pure gelatin and not Jell-O. The Jell-O gelatin contains a high amount of sugar.
2. For a large cupcake mold like the one used in this study heat 277 mL of distilled or deionized water to 180 °C on the hot plate.
3. If using a mold such as Morghan Alter's the cube molds 237 mL of distilled or deionized water and X grams of gelatin is used.
4. Mix 27.68 g of gelatin into the water continue heating and stirring for 10 minutes.
5. Let cool in beaker off hot plate for 30 minutes.
6. If using the cupcake mold tape or hot glue the plastic wrap on the base and make sure it is secure.

7. It is imperative that the gelatin mixture is cooled for these 30 minutes before pouring into the mold since many of the molds use a hot glued method and if not cooled it will destroy these glued connections.
8. Carefully pour into mold. Pour down the sides to mitigate air bubbles.
9. Let rest a minute or two to allow bubbles to begin floating to the top.
10. Take a piece of plastic wrap and carefully lay on surface it should be "sucked down" some because of the slight warmth.
11. Carefully peel off this take some of the surface air bubbles with it.
12. Place in fridge for 1- 2hrs to set uncovered (to let air bubbles escape) and use that day or the next morning. Letting it stay in the fridge too long or out too long can result and weird textures on the surface, so don't plan on molds lasting in fridge indefinitely.

Metamucil® Samples

From literature people have tried to incorporated mix-ins to help better mimic backscattering for imaging purposes and better estimate attenuation by providing elements that make the material more complex [36]. One such readily available mix-ins is sugar free Metamucil®. The small particulates provide backscatter which for imaging purposes is important to practice with to find a clear image of an organ. For the purposes of this study it helped provide more realistic attenuation. It was expected the samples with the Metamucil® would provide dampening effect to the ultrasound waves. The recipe was the same as the edible gelatin but 17.6 g of Metamucil® added. The water content was not equal for the edible gelatin samples and the gelatin #0 specimens, so the edible gelatin-Metamucil® sample was determined first and the gelatin 0# amount Metamucil® cut by half. The preliminary testing showed little change when the McGarry et. al recipe was used, so 2 tsp more of Metamucil® was added and this provided more dampening.

The Metamucil® for the edible gelatin specimen was mixed in following the 10 minutes mixing of gelatin powder and carefully avoided any clumps and cooled for 30 minutes and poured into the mold the same way as the edible gelatin. For the gelatin #0 mold following the 4 hrs. of melting the Metamucil® was carefully mixed in and all clumps taken care of and placed in the oven for another 3 hrs. Periodic checking on the Metamucil®-Gelatin #0 was performed with pushing the air bubbles to the side. Following the 3 hrs. any air bubbles remaining on the surface were pushed to the side to make a clear spot

in the center for the disc and probe. Following cooling this specimen had settled Metamucil® on the bottom which was consistent across all samples as the same techniques and amount was used.

Store-Bought Unflavored Gelatin Phantom with Sugar- Free Metamucil

1. Follow steps 1-4 and after gelatin is mixed add the 17.2 g of sugar free Metamucil and continue stirring until dissolved with no clumps. This mixture is normally dissolved in cold water, so watch for clumps and break up or filter out immediately. Takes about 3-4 minutes to get this dissolved.
2. Let cool 30 minutes.
3. Pour carefully in mold. Again, use the sides and watch for clumps when pouring use a strainer if necessary.
4. Let rest 2-3 minutes this time to allow more bubbles to reach the top.
5. Using a small piece of plastic wrap lay on the surface and remove the bubbles on top.
6. Place in fridge for 1- 2 hrs. to set and use that day or next morning.
7. Do not place in a part of the fridge that can freeze as this ruins the texture of the gelatin-Metamucil phantom and makes it unusable.

Ultrasound Testing

Ultrasound testing was performed using the Chattanooga Intelect TranSport machine. The frequency was set to 1 MHz a continuous duty cycle and intensity set to the max for this study of 1.0 W/cm^2. The petri dish with the disc was placed on a piece of Delrin that a thin textured silicone piece to help prevent sliding with a total height of X from the tabletop. The disc was then electrically connected to the resistance sweep circuit. The face of the ultrasound transducer was fixed using a vice and kept in contact parallel to the phantom surface by blue 3M tape to keep the probe from sliding upwards.

Figure 11 - Disc on petri dish with pork tissue compressed ontop of coupling gel and disc to ensure a good boundary.

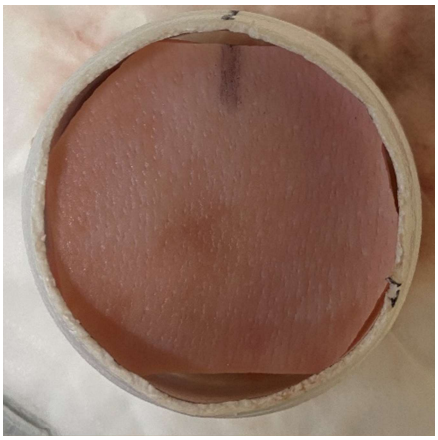

Figure 10 - Top view of pork specimen line indicates alignmint with the petri dish and the styrofoam cup for consistency between runs.

Figure 9 - Ultrasound Testing setup with probe fixed in vice and tape holding the transudcer face from rising up during testing by providing slight pressure.

Minimal pressure was applied with the tape to keep from applying abnormal pressure to the phantom. The goal was the keep the transducer in contact with the surface of the phantom to best mimic a clinical setting. The ultrasound was then turned on and disc and transducer repositioned to find the maximum output from the oscilloscope. Depending on how long this takes the first five 15 second runs are "warming up" and allow for repositioning and to let the ultrasound and disc warm up this was determined from the preliminary studies where the 5th data point was dropping and then steadily going up into the curve. The resistance sweep starting with a resistance on the box set to 20 ohms then begins with 15 seconds on and then 15 seconds off up to the 1510 ohm. With at total amount of time one equal to 4.5 minutes. This amount of time is safe for therapeutic ultrasound [45]. Following completion, the ultrasound is turned off and disc checked on the impedance capacitance resistance machine (LCR) to ensure connection is maintained and encapsulation is intact and 15 minutes to allow disc to "cool off." For each specimen 6 runs were performed and then averaged for that specimen. Any run where the probe slips or data points are not saved are left out and an additional run performed these are noted in lab notebook and raw data notes.

The porcine specimens could reach room temperature and measured using a thermocouple before the start of run 1. To preserve them they were placed in the refrigerator for the 15 minutes in between runs as was the edible gelatin specimens as they are not stable at room temperature for a long period of time. Once finished with testing the porcine tissues were wrapped in saline towels and placed in the freezer and the number of times thawed and frozen written down. A test run was performed with a "cold" sample below 70 degrees and this provided a smaller output which corresponds to a lower speed of sound in lower temperatures [46].

For the edible gelatin specimens, the plastic wrap acted as a barrier for the probe and coupling gel as coupling gel is water soluble and would create air bubbles if in direct contact with the edible gelatin specimens. Additionally, in preliminary studies when the disc became warm and there was a long period of time of the coupling gel in a slightly warmer environment with the Gelatin #0 small inclusions would begin to form in the Gelatin #0. To combat this a thermocouple was used for 6 runs and saw no increase and the cooling of 15 minutes in between was introduced. In addition, the coupling gel was carefully cleaned up around the disc area post run to help with it not sitting and possibly dissolving into the gelatin to create those inclusions.

Surface Area Estimation

The surface area of the sputter coated mesh was estimated 3 different ways. The first dividing the rectangle in half and treating it filament as a cylinder. Figure 27 shows one section of these diagonals. The lengths were measured and recorded. The surface area of the top and bottom of the cylinder were not accounted for as the sputter coater did not do the ends of the mesh. The estimation was to get the curve surface of one side of a cylinder. Thus, the formula utilized was πh.

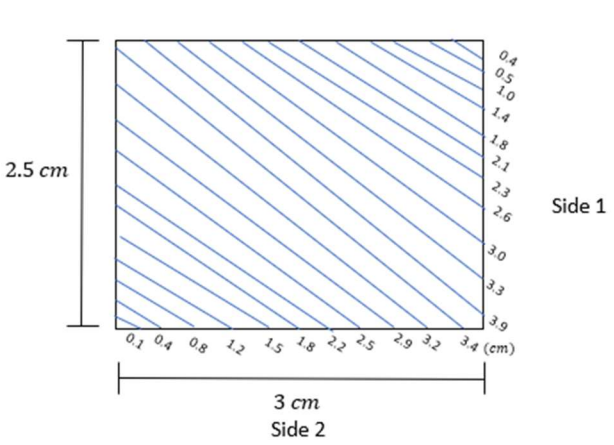

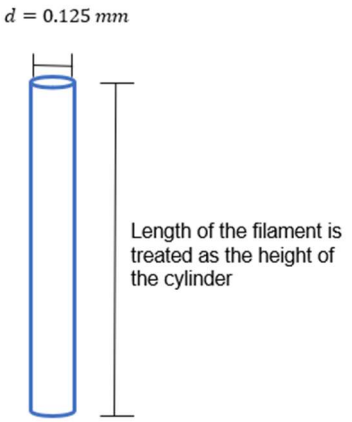

Figure 12 - Diagonal Filaments sketch. And filament modeled as a cylinder.

$$S.A.\ \ of\ a\ Cylinder = 2\pi r^2 + 2\pi h \qquad (1)$$

Equation 5 - Surface Area of a Cylinder

As this was one set of diagonals and the pattern is that of an open lap knit pattern the number of filaments was doubled to account for the over and under of the pattern. This number is then doubled for the addition direction of diagonals. The total area is then summed, and this is one half of the rectangle. This is then doubled for the full rectangle and used as the surface area for 1 well plate.

The next method of estimation used was taking a picture using the microscope and then using the help of a colleague and the software ImageJ to count the number of gold pixels per that unit area to determine the porosity percentage.

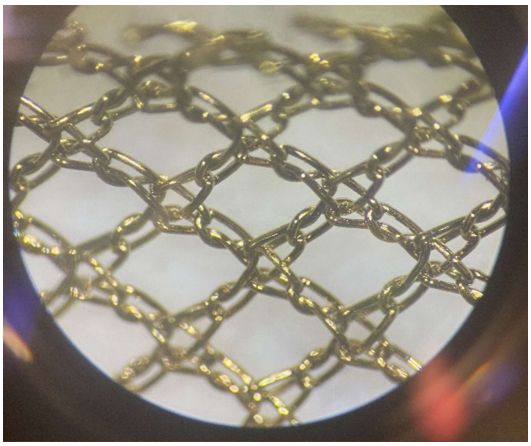

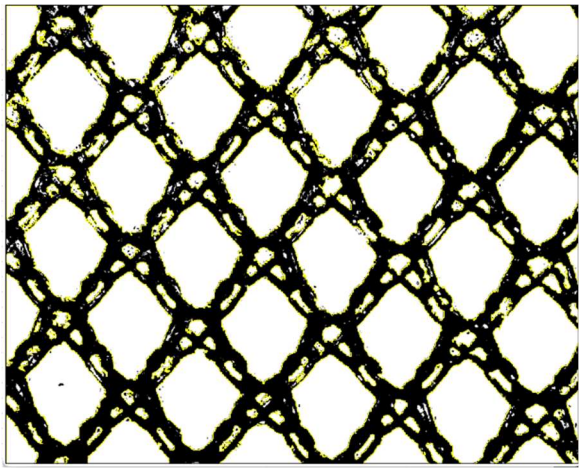

Figure 13 - ImageJ picture of mesh the highlighted portions are for the white space within the pores. The porosity can be found by using the white area divided by the total image area.

Lastly, a research paper examined the porosity of prosthetic meshes. Similar to hernia repair meshes there are a variety of types of prosthetic meshes used in cardiovascular implants, namely vascular prosthetics [47]. This paper used two different methods the first being weight and the next being area using topographical imaging. The area method was more precise and could be used for all mesh types. A similar type of mesh was used in this study, given their range of pore sizes and same knitting pattern the estimation is given in the table.

Table 6 - The porosity estimations. These can be used to determine the estimated surface area. Since the estimated measured surface area was close to the porosity from the paper with similar pattern this was used for the surface area calculations.

	Paper Estimation	**Measured and Calculated Estimation**	**ImageJ Estimation**
Porosity	60.10%	55.70%	40.00%

Table 7 - Area Estimations for each well. In addition, the total area given 6 wells.

Area per well plate (cm^2)	3.32
Total Area (cm2)	19.93

Sputter Coating

The material that is being applied is called a "target" and comes in many metallic forms. The free electrons flow from the negative source to the material in the plasma environment (where the plasma is seen to glow), these collide with the outer shell of Argon and due to their like charge, the inert gas with the + charged ions makes it attracted to the negatively charged material. This all occurs at a high velocity resulting in a "sputtering off" of the target material due to the momentum from the particle collisions. These particles then become deposited on the substrate in the vacuum chamber. Morgan Riley did the sputter coating using the sputter coater at the KU microscopy lab.

Appendix C: Data Processing Code

Single Disc Analysis MATLAB CODE

```
%% Main Analysis code for analyzation of ultrasound Single Disc PZT
% Written by Anna Norman
% Based on Luke Lindemann's code that was modified from Morghan Alters and originally Ember Krech.
%Last updated: 05/18/2021

clear;close all; clc;

%% Input Parameters
frequency = 1e6;
resistance_sweep=[20 50 80 100 150 200 250 300 350 400 500 600 700 800 1000 1200 1400 1500];
%resistance_sweep=[0 100 200 300];
%capacitance_sweep=[1e-6 0.68e-6 0.47e-6 0.33e-6 0.22e-6 0.15e-6 0.1e-6];

fc= 1.2e6; % cutoff frequency

%% File Reading

file_path = 'C:\Users\anorm\OneDrive\Documents\Hernia Repair\AN Thesis Raw Data\Gelatin 0-
Metamucil Specimens\Specimen 2 - new\1.0 SD Run 3\';   %file location the last part, "Data x.x stack" is
changed per data set

output_file=['7_21_Gelatin_0_Metamucil_2_Run_3_1.0_SD_10ohm'] ; % DP add DP at end if
differential probe was used
%check to see if voltage is scaled for the cable oscilloscope setup or
%unscaled for the differential probe setup in the equation section of code
for iResistor = 1:length(resistance_sweep)
    %for iCapacitor=1:length(capacitance_sweep)
    % resistance in parallel with capacitor
        %R1=10;
    % resistance the differential probe measures across to mimic muscle resistance
        Rmuscle=10;



    file_location=[file_path];
    data_file = ['tek39' num2str(iResistor+74,'%.2dCH1.csv')];    % need to add the file number example 15
was added b/c the file name is tek0116 this what the csv files are in each of those "0.5 DD or 0.5 SD
folders"
    input_name = [file_location data_file];
    data = dlmread(input_name,',',22,0);

    Rvar= resistance_sweep(iResistor); %resistance value in ohms
    %Cvar = capacitance_sweep(iCapacitor); %capacitor value in Farads

    %Time and voltage recording
```

```
time = data(:,1);                %seconds
voltage = data(:,2);              %volts
voltage =voltage-mean(voltage);    %center data around zero
raw_voltage(:,iResistor)=voltage;  %all raw voltage data

%Sample frequency claculation
deltaT= diff(time);               %sample freq
DeltaT = mean(deltaT);
fs=1/DeltaT;  %100Ms/sec 100 megasamples per second this is set on the o-scope
N=2^nextpow2(length(time));       %N points (2^n) for the FFT

%FFT and power spectrum calculation
dt=1/fs;                      %time between samples
range=(N/2);                  %range for the spectral plot
f=fs*(0:range-1)/N;           %frequency axis (starts at 0)

Y=fft(voltage);               %FFT using amount of data points recorded
Pyy=Y.*conj(Y)/N;             %Calculate the Power spectrum

   %PLOT the power spectrum of each data series
%      figure(1)
%      subplot(2,1,1)
%      plot(time,Y)
%      title('FFT')
%      xlabel('time (s)')
%      ylabel('Amplitude (V)')

%      hold on

%      subplot(2,1,2)
%      plot(f',Pyy(1:range))
%      title('Power Spectrum');
%      xlabel('Frequency (Hz)')
%      ylabel('V^2')

%       hold on

%filter
[b,a] = butter(5,2*fc/fs);        % (Nth order, cutoff frequency)how to determine cutoff freq
Vosc = filtfilt(b,a,voltage);

% Second FFT and power spectrum calculation AFTER lowpass filter

%      figure(2)
%      Y=fft(Vosc);              % FFT
%       Pyy=Y.*conj(Y)/N;        % Calculate the Power spectrum

%      subplot(2,1,1)
%      plot(time,Y)
%      title('FFT')
%      xlabel('time (s)')
```

```
%       ylabel('Amplitude (V)')

%       hold on

%       subplot(2,1,2)
%       plot(f',Pyy(1:range))
%       title('Power Spectrum');
%       axis ([0 100 0 .005]);
%       xlabel('Frequency (Hz)')
%       ylabel('V^2')

%        hold on

 % Variable calculations for voltage and power
    % most prevalent frequency from the PZT, found from the FFT and high
    % pass filter
    %fcc = 6.1e5;
    %C_impedance = 1./(2*pi*Cvar*fcc);               %equivalnce of capacitor resistance, non-imaginary
number
    %C_R1_eq = C_impedance*R1./(C_impedance+R1);          % equivalent impedance of the capacitor
and 10 ohm resistor in parallel
    R_total =Rvar+Rmuscle;                    %total impedance of the ciruit
  Vosc = voltage.*(1/sqrt(2));                        % convert to RMS voltage
  Vout = Vosc.*((1+(Rvar/Rmuscle)));          % scale voltage by the applied resistance - find voltage
produced by the specimen
  %Vout=Vosc;                               %use when using the
  %differential probe and comment out the scaled voltage
  P = Vout.^2./(Rvar+Rmuscle);          % instantaneous power of circuit

  %plot P vs Vosc (rms voltage)



  Pavg = trapz(time,P) * 1./(max(time) - min(time));      % average power
  Vpp = (max(raw_voltage(:,iResistor)) - (min(raw_voltage(:,iResistor))));
   Vamp = Vpp./2; % amplitude of voltage
   Vrms = Vamp.*(1/sqrt(2)); % Vrms Measured for the voltage drop across the 10ohm resistor



    %Vout=Vosc;   % unscaled voltage                    %because we used a differential probe I don't think it
needs to be scaled, but scaled before power of the circuit is calculated
                                                                %since the probe measured the actual voltage
drop across that resistor. This is used in the next line to find Vpp
    %Vpp = (max(Vout) - min(Vout));                % peak-to-peak voltage (amplitude)

    Pmax = Vrms.^2./(R_total);                      % peak power per cycle
    Pmaxu = Pmax*(10^6);
    Pmuscle_max = (Vrms.^2./Rmuscle).*10^6;                  % instantaneous power of muscle resistor

%% Store data to output
```

```
output(iResistor,:)={R_total, Vamp, Vpp, Pavg, Pmaxu, Vrms, Pmuscle_max};


   %end
end

%% Output to an excel sheet for later analysis
output_header = {'Resistance (ohm)' 'Voltage Amplitude (V)' 'V P-P (V)' 'Pavg (W)' 'Pmax (uW)' 'Vrms
(V)' 'Pmuscle_max (uW)'};

output = [output_header; output];

  xlswrite([output_file '.xls'], output_header,1,'A1')
  xlswrite([output_file '.xls'],output(2:length(resistance_sweep)+1,:),'Sheet1','A2')


disp('Done')
```

Statistical Analysis SAS Code

```
/*Single and Double disc ultrasound analysis with different tissue mimicking phantoms
Writen by Anna Norman
Modified from code written by Morghan Alters
Last updated: 07/27/2021 */

/*clear log */
dm 'log;clear';
/*clear output*/
dm 'output;clear';
/* Change the data file for each statistical analysis (21 different ones used) */
PROC IMPORT OUT=WORK.FROMXL
                        DATAFILE="C:\Users\a257l685\Documents\Avg Voltage.xls"
                        DBMS=XLS REPLACE ;
        SHEET="P-EGM";
        GETNAMES=YES;

RUN;
PROC PRINT DATA=FROMXL;

RUN;

/*Proc print to see all the data inputted. This includes all five specimens of each group and their power values with
each resistance for all 6 runs

/*============================================================
checking assumptions/requirements (START)
============================================================*/
*running 1-way model;
*this will allow a Normality test/plots, as well as an HOV plot (no test);
PROC GLM DATA=FROMXL;
```

```
CLASS Group ;
MODEL Average_Maximum_Voltage = Group;
MEANS Group ;
OUTPUT OUT=junk PREDICTED=yhat RESIDUAL=e;
QUIT;
PROC UNIVARIATE DATA=junk NORMAL PLOT;
VAR e;
RUN;
/*Plot the residuals vs predicted-y value to assess the homogeneity of variance assumption*/
PROC SGPLOT DATA=junk;
SCATTER Y=e X=yhat;
RUN;
/*Transforms the dependent variable in order to achieve the normality of residuals and homogeneity of
variance assumptions */
DATA FROMXL;
SET FROMXL;
Power_log = log(Average_Maximum_Voltage);
RUN;

PROC GLM DATA=FROMXL;
CLASS Group ;
MODEL Power_log = Group;
MEANS Group ;
OUTPUT OUT=junk PREDICTED=yhat RESIDUAL=e;
QUIT;
PROC UNIVARIATE DATA=junk NORMAL PLOT;
VAR e;
RUN;
/*Plot the residuals vs predicted-y value to assess the homogeneity of variance assumption*/
PROC SGPLOT DATA=junk;
SCATTER Y=e X=yhat;
RUN;

/*Checking assumptions for normality and equal variance complete. Next section of code is tukey-kramer post-hoc,
do determine the effect of phantom on power output.*/

PROC GLM DATA=FROMXL;
CLASS Group;
MODEL Power_log = Group;
Output OUT=junk PREDICTED=yhat RESIDUAL = e;
LSMEANS Group / CL LINES PDIFF=All ADJUST=TUKEY ALPHA=0.05;
QUIT;
```